IEEE Journal of Microwaves

Received 23 April 2021; revised 30 May 2021; accepted 30 May 2021. Date of publication 25 June 2021; date of current version 7 July 2021.

Digital Object Identifier 10.1109/JMW.2021.3085868

Photonic Generation of Wideband Chirped Microwave Waveforms

HAO CHI [1] (Senior Member, IEEE), CHAO WANG [2] (Senior Member, IEEE), AND JIANPING YAO [3] (Fellow, IEEE)

(Invited Paper)

[1]School of Communication Engineering, Hangzhou Dianzi University, Hangzhou 310018, China
[2]School of Engineering and Digital Arts, University of Kent, Canterbury CT2 7NT, U.K.
[3]School of Electrical Engineering and Computer Science, University of Ottawa, Ottawa, ON K1N 6N5, Canada

CORRESPONDING AUTHOR: Jianping Yao (e-mail: jpyao@uottawa.ca).

The work of Hao Chi was supported by the National Key R&D Program of China under Grant 2019YFB2203204, in part by the National Natural Science Foundation of China under Grant 61975048, and in part by the Zhejiang Provincial Natural Science Foundation under Grant LZ20F010003. The work of Chao Wang was supported by the Engineering and Physical Sciences Research Council of U.K. under Grant EP/S005625/1, and in part by the RCUK Catapult RiR programme under Grant EP/T51732X/1. The work of Jianping Yao was supported by the Natural Sciences and Engineering Research Council of Canada (NSERC).

ABSTRACT A chirped microwave waveform with a large time-bandwidth product (TBWP) can find important applications in modern radar systems and microwave imaging systems. Microwave photonics, a field that studies the generation and processing of microwave signals in the optical domain to take advantage of the ultra-wide bandwidth offered by photonics, has been considered an effective solution for high-frequency and large-bandwidth microwave waveform generation. In this paper, an overview on photonic generation of wideband chirped microwave waveforms is provided. Three major methods are discussed including chirped microwave waveform generation based on spectral shaping and frequency-to-time (SS-FTT) mapping, frequency and bandwidth multiplication, and Fourier-domain mode-locking of an optoelectronic oscillator (OEO). The performance of the techniques for chirped microwave waveform generation is studied. Techniques to generate chirped microwave waveforms based on photonic integrated circuits (PICs) are also discussed.

INDEX TERMS Microwave photonics, chirped microwave waveform, arbitrary waveform generation, time bandwidth product, optoelectronic oscillator.

I. INTRODUCTION

Pulse compression is a technique to increase the range resolution while relieving its constraint on peak power, which has widely been used in modern radar systems [1], [2]. In a pulse compression radar, the transmitter sends a microwave pulse with a large time-bandwidth product (TBWP) generated usually through frequency modulation or phase coding. The received echo signal is sent to a matched filter by which pulse compression is implemented [3]. The temporal width of a compressed pulse is approximately equal to the reciprocal of the bandwidth of the transmitted microwave pulse. The improvement in signal-to-noise ratio (SNR) through pulse compression is identical to the pulse compression ratio (PCR), which is the ratio of the uncompressed pulse width to the compressed pulse width. The PCR is approximately equal to its TBWP, which is the product of the temporal duration and the spectral bandwidth of an uncompressed pulse. Therefore, a pulse with a large TBWP means a large PCR, which would lead to a high range resolution. The TBWP could be as large as 10^5 or even greater in a pulse compression radar system [1]–[4].

To increase the TBWP, a microwave pulse should have a long temporal duration and a wide spectral width, which can be achieved through frequency modulation or phase coding. A microwave pulse with linear frequency modulation, also called as linearly chirped microwave pulse, is widely used in radar systems due to the key advantages including high tolerance to Doppler effect and relatively low complexity in the pulse generation and compression. A linearly chirped microwave pulse or waveform is conventionally generated electronically by a voltage-controlled oscillator (VCO) [5] or by an arbitrary waveform generator (AWG) [6]. A

chirped microwave waveform can also be generated in a passive manner. For example, by exciting a dispersive delay line, such as a surface acoustic wave delay line, with a microwave impulse, a linearly chirped microwave waveform is generated [7]. The major difficulty associated with the above electronics-based techniques is that the bandwidth of the generated microwave waveform is small, normally lower than a few gigahertz, making the TBWP small. This is due to the limited bandwidth of the electronic devices used, such as a VCO and a surface acoustic wave delay line, or the limited sampling rate of an AWG. However, for many wideband applications, such as in modern radar systems and next generation wireless communications systems, chirped microwave waveforms with a center frequency up to tens or even hundreds of gigahertz and a bandwidth of a few gigahertz or higher are often demanded [8]. In the past 20 years, great efforts have been directed to the search for effective solutions to generate high-frequency and large-bandwidth chirped microwave waveforms in the optical domain. Microwave photonics, a field that studies the generation and processing of microwave signals in the optical domain to take advantage of the ultra-wide bandwidth offered by photonics, has been considered an effective solution for high-frequency and wideband microwave waveform generation [9]–[15].

An early approach to the generation of a linearly chirped microwave waveform based on fiber optics was reported in 2005 [16], in which a linearly chirped microwave waveform was generated based on the coherent beating of two time-delayed linearly chirped optical pulses by passing an ultra-short optical pulse through two linearly chirped fiber Bragg gratings (LCFBGs) with different dispersion values. Since then, numerous photonic approaches for the generation of chirped microwave waveforms have been demonstrated. In this paper, an overview of the techniques proposed in the past 20 years for photonic generation of chirped microwave waveforms is provided. In particular, three major methods are discussed. The first method is based on spectral shaping and frequency-to-time (SS-FTT) mapping. The spectrum of an ultra-short optical pulse is modified to have a shape identical to that of a microwave waveform to be generated. Then, through FTT mapping and photodetection, a temporal microwave waveform is generated. The key component for linearly chirped microwave waveform generation is the spectral shaper which should have a spectral response having a linearly changing free spectrum range (FSR). This can be realized using a Mach-Zehnder interferometer (MZI) with one arm having a wavelength dependent arm length or a fiber Bragg grating (FBG) with a specially tailored spectral response. The second method is based on frequency multiplication, to multiply the frequency of an electronically generated chirped microwave waveform with a relatively low center frequency and narrow bandwidth. For a multiplication factor of N, the center frequency and the bandwidth are both increased by N times. Frequency multiplication can be implemented based on external modulation or photonic time compression (PTC). The third method is to generate a wideband linearly

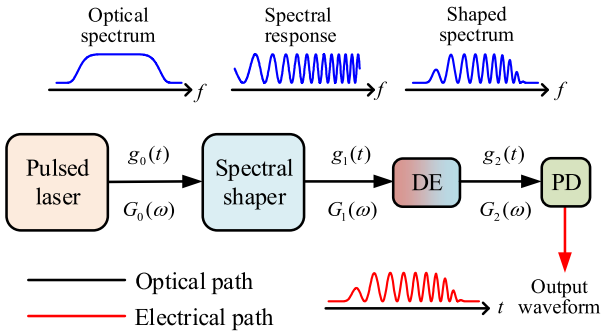

FIGURE 1. Photonic generation of a linearly chirped microwave waveform based on spectral shaping and frequency-to-time mapping (DE: dispersive element; PD: photodetector).

chirped microwave waveform based on Fourier-domain mode locking of an optoelectronic oscillator (OEO). In a regular frequency-tunable OEO, the oscillation, when being tuned from one frequency to another, will need a buildup time to stabilize the oscillation at the new frequency, making the generated frequency-tuned microwave waveform have high phase noise. A Fourier-domain mode locked (FDML) OEO, on the other hand, is able to generate a highly coherent linearly chirped microwave waveform with a low phase noise since all oscillation modes are phase locked and coexist in the cavity, the tuning from one mode to another does not change the phase relationship between the modes and will not create additional phase noise. All the methods reported are implemented based on discrete components. To reduce the size and cost, photonic integration is highly needed. In this paper, techniques to generate linearly chirped microwave waveforms based on photonic integrated circuits (PICs) will also be discussed.

II. CHIRPED MICROWAVE WAVEFORM GENERATION BASED ON SS-FTT MAPPING

The first method for photonic generation of a linearly chirped microwave waveform is based on SS-FTT mapping. In such a system, an ultrashort optical pulse from a pulsed laser, such as a mode-locked laser, is spectrally tailored by a spectral shaper whose frequency response is designed to have a shape identical to that of a microwave waveform to be generated. For example, to generate a linearly chirped microwave waveform, the spectral shaper should have a sinusoidal spectral response with a linearly changing FSR. After passing through the spectral shaper, the ultra-short pulse is spectrally shaped, which is sent to an optical dispersive element (DE) to perform FTT mapping. To have a linear FTT mapping, a DE with linear dispersion is needed [16]–[48]. The generation process is illustrated in Fig. 1. As can be seen, an ultra-short pulse with a broad spectrum generated by a mode locked laser source is send to a spectral shaper with a spectral response having a linearly increasing or decreasing FSR [49], the spectrum-shaped optical pulse is then sent to a DE where FTT mapping is performed, leading to the generation of a temporal waveform that as a shape identical to the spectrum of the spectrum-shaped

pulse. After photodetection, the optical pulse is converted to a microwave pulse. Note that the locations of the spectral shaper and the DE in the system can be interchanged since both the spectral shaper and FTT mapping element are linear devices.

A. PRINCIPLE OF FREQUENCY-TO-TIME (FTT) MAPPING

There is a well-known space-time duality between the paraxial diffraction of a light beam in space and the chromatic dispersion of a short pulse in time, which can be used to create time-domain counterparts of spatial optical systems, such as time lens, temporal imaging, and temporal Talbot effect [50]–[52]. FTT mapping, also known as wavelength-to-time mapping, comes from the property of real-time Fourier transform of a short pulse passing through a DE, which can be understood as the time-domain Fraunhofer diffraction [49]. In a system shown in Fig. 1, a short pulse with its time-domain and frequency-domain complex envelopes $g_0(t)$ and $G_0(\omega)$, is first spectrally shaped by a spectral shaper. The spectrum-shaped pulse, denoted as $g_1(t)$ and $G_1(\omega)$ in the time and frequency domains, respectively, is sent to a DE, which has a first-order dispersion $\ddot{\Phi}$ (in ps^2, defined as the derivative of the group delay with respect to the angular frequency). A time-domain waveform $g_2(t)$ is generated at the output of the DE, which is a copy of the spectrum $G_1(\omega)$ before the DE.

For simplicity without loss of generality, we assume that the input ultra-short pulse is a transform-limited Gaussian pulse. Its time-domain and frequency-domain complex envelopes are given by

$$g_0(t) = \exp\left(-\frac{t^2}{2\tau_0^2}\right) \tag{1}$$

and

$$G_0(\omega) = \mathfrak{F}\{g_0(t)\} = \sqrt{2\pi}\tau_0 \exp\left(-\frac{{\tau_0}^2\omega^2}{2}\right) \tag{2}$$

respectively, where τ_0 denotes the half width at $1/e$ peak intensity of the pulse and $\mathfrak{F}\{\cdot\}$ denotes the Fourier transform. The spectrum of the spectrum-shaped pulse is given by $G_1(\omega) = G_0(\omega) \cdot H_f(\omega)$, where $H_f(\omega)$ denotes the frequency response of the spectral shaper. The frequency response of the DE is given by $H_D(\omega) = \exp(-j\frac{1}{2}\ddot{\Phi}\omega^2)$, in which the loss and the frequency-independent group delay induced by the DE are ignored. If the far-field condition is satisfied, or in other words, the time width Δt_1 of $g_1(t)$ is sufficiently small and the dispersion amount $\ddot{\Phi}$ is sufficiently large such that

$$\left|\frac{\Delta t_1}{2\pi\ddot{\Phi}}\right| << 1 \tag{3}$$

the optical pulse at the output of the DE can be approximated by

$$g_2(t) = C\mathfrak{F}\{g_1(t)\}|_{\omega=t/\ddot{\Phi}} = CG_0\left(\frac{t}{\ddot{\Phi}}\right)H_f\left(\frac{t}{\ddot{\Phi}}\right) \tag{4}$$

where C is a constant [49].

Under the far-field condition given by Eq. (3), the envelope of the output pulse is a scaled Fourier transform of the spectrum-shaped pulse $g_1(t)$ with a shape identical to the spectrum $G_1(\omega)$, which means a linear mapping from the spectrum of a pulse to the time domain to get a temporal waveform is realized. Fig. 2 schematically shows the FTT mapping process. In order to visualize the relationship between the input and output pulses in the time and frequency domains, the input pulse is assumed to be a rectangular function and the output pulse is thus a Sinc function. After photodetection, the optical waveform is converted into an electrical waveform. Note that the electrical current after a photodetector (PD) is proportional to the intensity of the output pulse, given by $i(t) \propto |g_2(t)|^2$, due to the square-low detection of a PD.

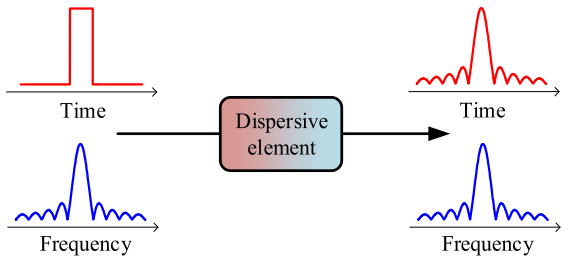

FIGURE 2. Schematic illustration of the frequency-to-time mapping.

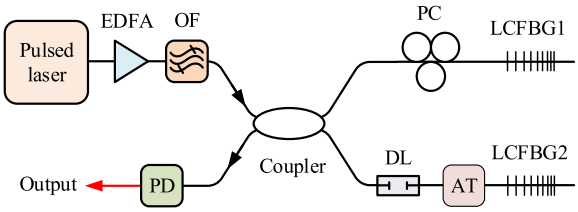

FIGURE 3. Photonic generation of a linearly chirped microwave waveform using a pair of LCFBGs with slightly different chirp rate (EDFA: erbium-doped fiber amplifier; OF: optical filter; PC: polarization controller; CFBG: chirped fiber Bragg grating; DL: delay line; AT: attenuator; PD: photodetector) [16].

B. SPECTRAL SHAPER BASED ON FIBER OPTICS [16]–[23]

The key device in an SS-FTT mapping system is the spectral shaper, which should have a spectral response with the same shape as the waveform to be generated. A simple approach to implement such a spectral shaper is to use an MZI with one arm having a wavelength dependent arm length. Thanks to the wavelength dependent time delay difference, the FSR is not fixed, but changing linearly with respect to the wavelength. Fig. 3 shows an MZI with a time delay difference that is wavelength dependent [16]. As can be seen, two linearly chirped FBGs (LCFBGs) with different chirp rates are placed in the two arms of the MZI. A tunable optical delay line is incorporated in one arm to control the relative time delay and an attenuator is employed to balance the optical powers of the two arms, to control the contrast ratio of the spectral response. The spectral response has an FSR that is wavelength dependent. When an ultra-short optical pulse is launched into the MZI, the spectrum of the ultra-short pulse is tailored to have a shape identical to that of the spectral response of the MZI. The shaped spectrum is also mapped to the time domain

due to the dispersion of the LCFBGs. After photodetection at the PD, a linearly chirped microwave waveform is generated.

The analysis of the system in Fig. 3 can be performed based on the principle of SS-FTT mapping given in Section II-A, but the configuration is slightly different from the one shown in Fig. 1. In Fig. 1, the SS-FTT mapping is performed by two independent devices. Here in Fig. 3, the two functions are performed by the two LCFBGs. In fact, the two LCFBGs have two roles, serving as wavelength-dependent delay lines in the two arms of the MZI to introduce wavelength dependent time delay difference, making the MZI have a wavelength dependent FSR, and serving as a DE to perform FTT mapping.

In fact, the waveform generation process can also be explained based on an interferometry approach, in which two linearly chirped optical pulses are generated by applying an ultra-short pulse to the LCFBGs to generate two linearly chirped optical waveforms. By beating the two linearly chirped optical waveforms at a PD, a linearly chirped microwave waveform is generated.

Assume the dispersion values of the two LCFBGs are $\ddot{\Phi}_1$ and $\ddot{\Phi}_2$, and the input pulse is a transform-limited Gaussian pulse as given in Eq. (1). If the far-field condition is satisfied, the optical pulses reflected from the two LCFBGs in the time domain are

$$g_j(t) = \frac{\tau_0}{\sqrt{|\ddot{\Phi}_j|}} \exp\left(-\frac{t^2}{2\tau_j^2}\right), j = 1, 2 \tag{5}$$

where $\tau_j (j = 1, 2)$ denotes the temporal width of the reflected pulses. The two pulses are combined and beat at the PD. The photocurrent at the output of the PD is given by

$$\begin{aligned} i(t) \propto |g_1(t)|^2 + |g_2(t+\delta t)|^2 \\ + 2\,|g_1(t)|\,|g_2(t+\delta t)| \cos\left[\frac{t^2}{2\ddot{\Phi}_1} - \frac{(t+\delta t)^2}{2\ddot{\Phi}_2}\right] \end{aligned} \tag{6}$$

where δt is the time delay difference between the two reflected pulses introduced by the delay lines. The instantaneous angular frequency of the waveform is given by

$$\omega(t) = \frac{\mathrm{d}\varphi}{\mathrm{d}t} = \left|\left(\frac{1}{\ddot{\Phi}_1} - \frac{1}{\ddot{\Phi}_2}\right) t - \frac{\delta t}{\ddot{\Phi}_2}\right|. \tag{7}$$

As can be seen the instantaneous frequency of the generated waveform varies linearly with time. The chirp rate is determined by the dispersion amounts of the two LCFBGs and the relative time delay δt can be used to adjust the center frequency of the generated chirped microwave waveform.

Now we estimate the TBWP of the generated microwave waveform. The bandwidth of the LCFBGs is denoted by Δf_{opt}. The coherent superposition of the two reflected pulses requires that the two pulses overlap in time as much as possible, which means the dispersion amounts $\ddot{\Phi}_1$ and $\ddot{\Phi}_2$ should be almost the same, i.e., $\ddot{\Phi} = \ddot{\Phi}_1 \approx \ddot{\Phi}_2$, and the pulse widths of $g_1(t)$ and $g_2(t)$ should be far larger than their relative time delay δt. The temporal duration of the generated electrical pulse is estimated to be $\tau_{\text{rf}} = 2\pi\,\Delta f_{\text{opt}}|\ddot{\Phi}|$. The bandwidth can be calculated according to the time duration and the chirp rate of the generated pulse given in Eq. (7), which is obtained

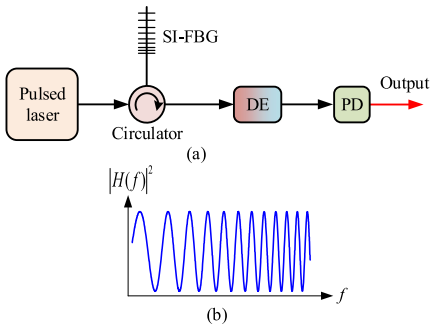

FIGURE 4. (a) Photonic generation a linearly chirped microwave waveform using an SI-FBG as a spectral shaper (PD: photodetector; SI-FBG: superimposed FBG; DE: dispersive element) [18]; (b) typical power spectrum of a SI-FBG with two LCFBGs having different chirp rates.

and given by $\Delta f_{\text{rf}} = |\frac{1}{\ddot{\Phi}_1} - \frac{1}{\ddot{\Phi}_2}|\frac{\tau_{\text{rf}}}{2\pi}$. Therefore, the maximum TBWP is given

$$\text{TBWP}_{\max} = \Delta f_{\text{rf}} \cdot \tau_{\text{rf}} = 2\pi\,\Delta f_{\text{opt}}{}^2 \Delta\ddot{\Phi} \tag{8}$$

where $\Delta\ddot{\Phi} = |\ddot{\Phi}_1 - \ddot{\Phi}_2|$. It is seen that the TBWP of the generated chirped microwave waveform is limited by the optical bandwidth and the dispersion difference of the two LCFBGs. For example, for the LCFBGs with a bandwidth of Δf_{opt}= 1000 GHz and a dispersion difference of $\Delta\ddot{\Phi}$= 20 ps^2, the maximum TBWP is estimated to be around 40π.

To avoid using two physically separated LCFBGs to make the system have better stability, Wang and Yao proposed to replace the two LCFBGs by a single superimposed FBG (SI-FBG) [18]. Due to the small dispersion of the SI-FBG, an additional DE was employed for implementing FTT mapping, as shown in Fig. 4(a) [18]. The SI-FBG consists of two spatially and spectrally overlapped LCFBGs with different chirp rates. A longitude offset between the two LCFBGs was introduced when fabricating the SI-FBG for generating a linearly chirped microwave waveform with a given center frequency. If the dispersion amounts of the two LCFBGs within the SI-FBG are $\ddot{\Phi}_1$ and $\ddot{\Phi}_2$, and the relative time delay between the reflected pulses induced by the longitude offset is δt, the power transfer function of the SI-FBG can be expressed as

$$|H_f(\omega)|^2 = 1 + \cos\left[\omega\delta t + \frac{1}{2}\left(\ddot{\Phi}_1 - \ddot{\Phi}_2\right)\omega^2\right]. \tag{9}$$

Again, there is a quadratic term in the cosine function, which indicates that a linearly varying FSR is in its spectral response, as shown in Fig. 4(b). According to the principle of FTT mapping, the microwave waveform at the output of the PD is

$$i(t) \propto \left|G_0\left(\frac{t}{\ddot{\Phi}_3}\right) H_f\left(\frac{t}{\ddot{\Phi}_3}\right)\right|^2$$

$$= \left|G_0\left(\frac{t}{\ddot{\Phi}_3}\right)\right|^2 \left\{1+\cos\left[\delta t\frac{t}{\ddot{\Phi}_3}+\frac{1}{2}\left(\ddot{\Phi}_1-\ddot{\Phi}_2\right)\left(\frac{t}{\ddot{\Phi}_3}\right)^2\right]\right\} \tag{10}$$

where $\ddot{\Phi}_3$ is the dispersion value of the additional DE. Note that Eq. (10) is obtained under the conditions of $|\ddot{\Phi}_3| >> |\ddot{\Phi}_1|, |\ddot{\Phi}_2|$ and $|\ddot{\Phi}_3/\tau_0| >> \delta t$(the far-field condition). The instantaneous angular frequency of the generated microwave waveform is calculated to be $\omega(t) = |\frac{\ddot{\Phi}_1-\ddot{\Phi}_2}{\ddot{\Phi}_3^2}t + \frac{\delta t}{\ddot{\Phi}_3}|$. Therefore, the chirp rate is determined by the dispersion amounts $\ddot{\Phi}_1$, $\ddot{\Phi}_2$ and $\ddot{\Phi}_3$, and the relative time delay δt is used to adjust the center frequency of the generated chirped microwave waveform.

Here we estimate the TBWP of the approach shown in Fig. 4. We assume the bandwidths of the two LCFBGs within the SI-FBG are identical and given by Δf_{opt}. The temporal duration the generated microwave waveform is calculated to be $\tau_{\text{rf}} = 2\pi\Delta f_{\text{opt}}|\ddot{\Phi}_3|$. The microwave bandwidth is $\Delta f_{\text{rf}} = \frac{\Delta\ddot{\Phi}\tau_{\text{rf}}}{2\pi|\ddot{\Phi}_3|^2}$ according to Eq. (10), where $\Delta\ddot{\Phi} = |\ddot{\Phi}_1 - \ddot{\Phi}_2|$. Therefore, the maximum TBWP that can be achieved is given by $\text{TBWP}_{\max} = \Delta f_{\text{rf}} \cdot \tau_{\text{rf}} = 2\pi\Delta {f_{\text{opt}}}^2\Delta\ddot{\Phi}$, which is the same as that in Eq. (8). It means that the maximum achievable TBWP is independent of the dispersion amount of the additional DE, but is solely determined by the parameters of the two LCFBGs (bandwidth and dispersion difference) within the spectral shaper. Despite that the temporal duration increases with the higher dispersion amount $|\ddot{\Phi}_3|$, the TBWP of the chirped microwave waveform does not increase accordingly since the bandwidth of the microwave waveform is inversely proportional to $|\ddot{\Phi}_3|$. In addition, if the two LCFBGs satisfy $\ddot{\Phi}_1 = -\ddot{\Phi}_2 = \ddot{\Phi}$, the maximum TBWP is calculated to be [19]

$$\text{TBWP}_{\max} = 4\pi\Delta {f_{\text{opt}}}^2\left|\ddot{\Phi}\right| = 2\Delta f_{\text{opt}}\Delta\tau = \left(\frac{4n_{eff}L}{c}\right)\Delta f_{\text{opt}} \tag{11}$$

where n_{eff} and L are the effective refractive index and length of the LCFBGs, respectively, c is the speed of light in vacuum, and $\Delta\tau$ is the differential group delay over a frequency span of Δf_{opt}. As can be seen, the length and the bandwidth of the LCFBGs determine the maximum TBWP. In other words, the maximum TBWP of the generated chirped microwave waveform is decided by the length bandwidth product of the LCFBGs used. For instance, if the length and bandwidth of the LCFBGs are $L = 1$ cm and $\Delta f_{\text{opt}} = 1000$ GHz, respectively, the upper limit of the TBWP is estimated to be around 400.

In the above SI-FBG based scheme, the longitude offset between the two LCFBGs within the SI-FBG is fixed once the SI-FBG is fabricated, which means the center frequency of the generated chirped waveform cannot be tuned. Wang and Yao proposed another FBG-based approach to generating a linearly chirped microwave waveform with tunable center frequency [19]. The spectral shaper is implemented based on a Sagnac loop mirror that incorporates an LCFBG with 100% reflection and a tunable delay line, as shown in Fig. 5. In this case, the power transfer function of the spectral shaper is similar to that in Eq. (9), but the relative time delay δt is tunable and $\ddot{\Phi}_1 = -\ddot{\Phi}_2$ since only one LCFBG operating in total reflection from both sides is employed.

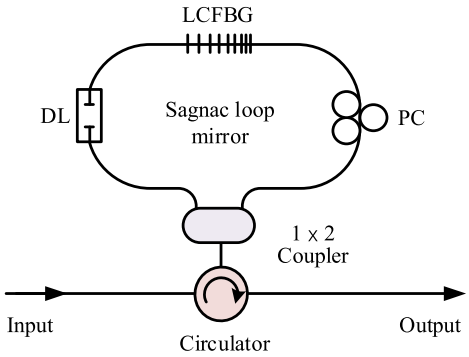

FIGURE 5. Spectral shaper based on a Sagnac loop mirror incorporating an LCFBG (LCFBG: linearly chirped fiber Bragg grating; DL: delay line; PC: polarization controller) [19].

One key advantage of using FBGs in the generation of chirped microwave waveforms lies in the fact that the required spectral shaper and DE can be realized using a single LCFBG. In [20], it was demonstrated that an arbitrary waveform, including a chirped microwave waveform, with a large TBWP can be generated based on SS-FTT mapping using a single spatially discrete LCFBG (SD-LCFBG). The SD-LCFBG was fabricated using a linearly chirped phase mask by axially shifting the photosensitive fiber to introduce a spatial spacing between two adjacent sub-gratings during the fabrication process. In [21], a method to generate a chirped microwave waveform with a continuously tunable chirp rate was proposed and demonstrated. In this approach, an optically pumped LCFBG, which was written in an erbium-ytterbium co-doped fiber, is incorporated in one arm of an MZI. The tuning of the chirp rate can be realized by pumping the LCFBG with different pumping power. The major advantage of the approach is that the tuning is implemented in an all-fiber manner and can be controlled at a remote site.

Instead of using FBGs, an optical dispersive fiber, such as a standard single-mode fiber or a dispersion compensating fiber, can be employed to serve as not only a DE for FTT mapping but also a spectral shaper [22]–[23]. Similar to the MZI in Fig. 3, where two LCFBGs were employed, an MZI with a dispersive fiber in one arm, shown in Fig. 6, can also be used as a spectral shaper with a linearly varying FSR [23]. A second dispersive fiber is employed as a DE to implement FTT mapping. The length difference between the two arms in this MZI is large and can be adjusted by using a tunable time delay line. Due to the chromatic dispersion of the first dispersive fiber, the MZI has a spectral response with its FSR that is wavelength dependent.

The power transfer function of the MZI is given by

$$\left|H_f(\omega)\right|^2 = 1+\cos\left(\omega\delta t+\frac{1}{2}\ddot{\Phi}_1\omega^2\right) \tag{12}$$

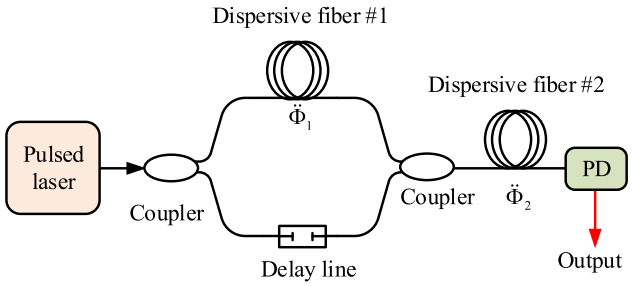

FIGURE 6. Spectral shaper based on a dispersive fiber for the generation of a linearly chirped microwave waveform [23] (PD: photodetector).

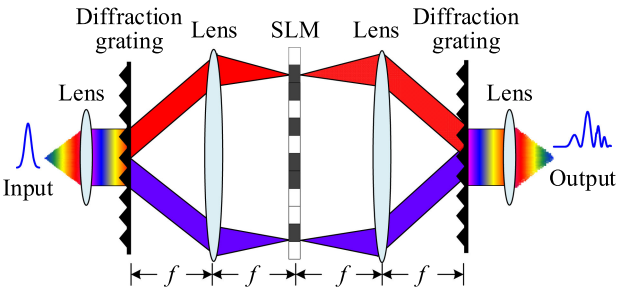

FIGURE 7. Schematic diagram of a programmable spectral shaper based on a spatial light modulator (SLM).

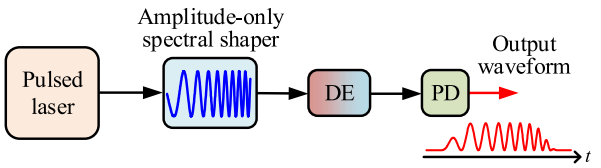

FIGURE 8. Chirped microwave waveform generation using an amplitude-only spectral shaper based on a spatial light modulator (SLM) (DE: dispersive element; PD: photodetector).

where $\ddot{\Phi}_1$ is the dispersion amount of the dispersive fiber within the MZI and δt is the relative time delay between the two arms. Assume the dispersion value of the second dispersive fiber is $\ddot{\Phi}_2$ and $|\ddot{\Phi}_1| << |\ddot{\Phi}_2|$, the microwave waveform at the output of a PD is given by

$$i(t) \propto \left|G_0\left(\frac{t}{\ddot{\Phi}_2}\right)\right|^2 \left\{1+\cos\left[\delta t\left(\frac{t}{\ddot{\Phi}_2}\right)+\frac{1}{2}\ddot{\Phi}_1\left(\frac{t}{\ddot{\Phi}_2}\right)^2\right]\right\} \tag{13}$$

and the instantaneous frequency is given by

$$\omega(t) = \left|\left(\frac{\ddot{\Phi}_1}{\ddot{\Phi}_2^2}\right)t + \left(\frac{\delta t}{\ddot{\Phi}_2}\right)\right|. \tag{14}$$

Similarly, the maximum TBWP of the generated chirped microwave waveform is given by

$$\mathrm{TBWP}_{\max} = \Delta f_{\mathrm{opt}} \cdot \tau_{\mathrm{rf}} = 2\pi \Delta {f_{\mathrm{opt}}}^2 \left|\ddot{\Phi}_1\right| \tag{15}$$

Since the bandwidth of the dispersive fiber in the upper arm is much greater than that of an LCFBG, the bandwidth of the generated microwave waveform is dependent only on the bandwidth of the ultra-short pulse and that of the PD. Therefore, in theory, the maximum TBWP is far greater than that using a FBG-based spectral shaper. However, the employment of a long dispersive fiber (to achieve the required large dispersion) would make the system have a large size, reduced stability, and increased attenuation. To compensate for the loss, power amplification is needed, which may lead to amplifier-induced noise, making the generated microwave waveform have poorer SNR.

C. SPECTRAL SHAPER BASED ON FREE SPACE OPTICS [24]–[32]

Spectral shapers can also be implemented based on free space optics. The key device in a free-space-based spectral shaper is a spatial light modulator (SLM), which is able to shape the spectrum of an input optical pulse at a high speed (a typical response time of 10∼100 ms). The potential of using SLMs for arbitrary waveform generation has been well studied [15]. Fig. 7 shows an SLM-based spectral shaper, which is a well-known 4f system. As can be seen the system consists of a pair of collimating lenses, a pair of diffraction gratings, a pair of Fourier lenses, and an SLM placed between the two Fourier lenses [24]. An incident ultra-short optical pulse, after passing through the first collimating lens, is diffracted by the first diffraction grating to separate the colors (or wavelengths) and sent to the SLM through the first Fourier lens. The amplitude and/or phase of the spatially dispersed spectral components is then modulated (or shaped) by the SLM, which can operate in either the transmission or reflection mode. The spectrally shaped spectral components are sent to the second diffraction grating through the second Fourier lens, where the separated colors are recombined. A temporal waveform is then obtained at the output of the second collimating lens. To generate a specific microwave waveform, the SLM should be reconfigured to have a spatial pattern that is a scaled version of the temporal waveform. The state-of-the-art SLMs based on liquid crystal on silicon have been widely used in performing spectral shaping due to its advantages of good compactness and high resolution.

For linearly chirped microwave waveform generation, the SLM can be configured to operate as an amplitude-only spectral shaper with a pre-designed linearly chirped spatial pattern. With the help of a DE, the spectrum after spectral shaping can be mapped to the time domain to generate a linearly chirped microwave waveform, as shown in Fig. 8 [25, 27].

Mathematically, to generate a linearly chirped microwave waveform, the spectral shaper should have a spectral response given by [27]

$$H(\omega) = \left|\cos\left(t_0\omega + \frac{1}{2}K\omega^2\right)\right| \tag{16}$$

where t_0 and K are parameters determining the center frequency and chirp rate of the generated chirped microwave waveform. After passing through a DE with a dispersion value

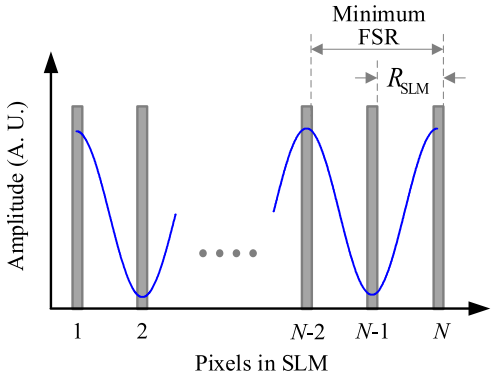

FIGURE 9. Sinusoidal pattern recorded in an SLM with a minimum achievable free spectral range (FSR).

of $\ddot{\Phi}$, we have a time-domain waveform as

$$i(t) \propto \left|G_0\left(\frac{t}{\ddot{\Phi}}\right)\right|^2 \left[1+\cos\left(\frac{2t_0}{\ddot{\Phi}}t+\frac{K}{\ddot{\Phi}^2}t^2\right)\right] \tag{17}$$

From (17), the instantaneous angular frequency of the generated chirped microwave waveform can be calculated by $\omega = 2t_0/\ddot{\Phi} + 2Kt/\ddot{\Phi}^2$. It is linearly chirped, the center frequency is $\omega_c = 2t_0/|\ddot{\Phi}|$, and the chirp rate is $C = K/(\pi\ddot{\Phi}^2)$.

Different from an FBG-based spectral shaper, the liquid crystal SLM-based spectral shaper has limited frequency resolution due to the discrete nature (with finite number of pixels) of an SLM. We assume that the frequency resolution of an SLM is R_{SLM}, the bandwidth Δf_{opt} of the spectral shaper is given by $\Delta f_{opt} = R_{SLM} \cdot N$, where N is the pixel number of the SLM in one dimension. Note that the frequency resolution R_{SLM} is defined as the half of the minimum achievable FSR of the sinusoidal pattern given in Eq. (16) that can be recorded in the spectral shaper according to the sampling theorem, as shown in Fig. 9. According to the principle of FTT mapping ($\omega \Leftrightarrow t/\ddot{\Phi}$) given in Eq. (4), the frequency resolution R_{SLM} decides the minimum period of the generated waveform, which is given by $2\pi R_{SLM}|\ddot{\Phi}| = T_{min}/2$. In other words, the maximum instantaneous frequency f_{max} of a generated microwave waveform is given by $f_{max} = 1/(4\pi|\ddot{\Phi}|R_{SLM})$, which can be used to estimate the maximum bandwidth Δf_{rf} of the generated chirped microwave waveform. The temporal duration of the waveform can be calculated according to the spectral width and the dispersion amount, which is given by $\tau_{rf} = 2\pi\Delta f_{opt}|\ddot{\Phi}|$. Therefore, the maximum TBWP that can be achieved is given by [29],

$$\mathrm{TBWP}_{max} = \Delta f_{rf} \cdot \tau_{rf} = \frac{2\pi\Delta f_{opt}\left|\ddot{\Phi}\right|}{4\pi\left|\ddot{\Phi}\right|R_{SLM}} = \frac{\Delta f_{opt}}{2R_{SLM}} = \frac{N}{2} \tag{18}$$

It is seen that the maximum achievable TBWP is limited by the pixel number of the SLM (in one dimension) within the spectral shaper. For an SLM with a typical pixel number $N = 2000$, the upper limit of the TBWP is 1000. In a system with appropriately chosen parameters (pulse width, pattern recorded in an SLM and dispersion amount), the TBWP of a generated chirped microwave waveform can be close to the above upper limit. Note that the maximum TBWP is estimated by considering a chirped microwave waveform with its instantaneous frequency spanning from DC to its maximum oscillating frequency, which means the actual upper-limit TBWP is less than $N/2$ if one aims to generate a chirped microwave waveform with the lowest frequency greater than zero. For example, if a chirped microwave waveform to be generated has an instantaneous frequency spanning from 30 to 40 GHz, the actual upper limit of the TBWP is $N/8$. In addition, some works also showed that the far-field condition given by Eq. (3) can be relaxed, leading to a much smaller dispersion required to perform FTT mapping. Studies about the relaxed far-field condition can be found in [31]–[32].

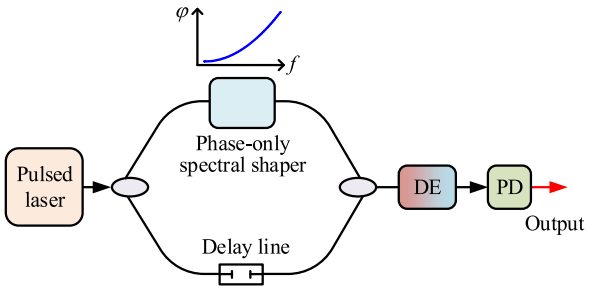

FIGURE 10. Chirped microwave waveform generation with a phase-only spectral shaper in a Mach-Zehnder interferometer (DE: dispersion element; PD: photodetector).

A phase-only spectral shaper can also be used to generate a chirped microwave waveform. By incorporating a phase-only spectral shaper in one arm of an MZI, as shown in Fig. 10, a spectral response of the MZI with a linearly increasing or decreasing FSR is obtained [29]–[30]. By using a DE to perform FTT mapping, a linearly chirped microwave waveform is generated. The phase response of the spectral shaper is given by $\varphi = k\omega^2$, where k is a constant denoting the phase modulation coefficient. Therefore, the transfer function of the MZI is given by

$$H(\omega) = \exp(-j\omega\delta t) + \exp(jk\omega^2) \tag{19}$$

where δt denotes the time delay difference between the two arms of the MZI. According to the principle of FTT mapping, the microwave waveform generated at the output of the PD is as

$$i(t) \propto \left|G_0\left(\frac{t}{\ddot{\Phi}}\right)\right|^2 \left\{1+\cos\left[\delta t\left(\frac{t}{\ddot{\Phi}}\right)+k\left(\frac{t}{\ddot{\Phi}}\right)^2\right]\right\} \tag{20}$$

where $\ddot{\Phi}$ is, again, the dispersion value of the DE after the MZI. Therefore, the instantaneous angular frequency can be calculated by

$$\omega(t) = \frac{\delta t}{|\ddot{\Phi}|} + \left(\frac{2k}{\ddot{\Phi}^2}\right)t. \tag{21}$$

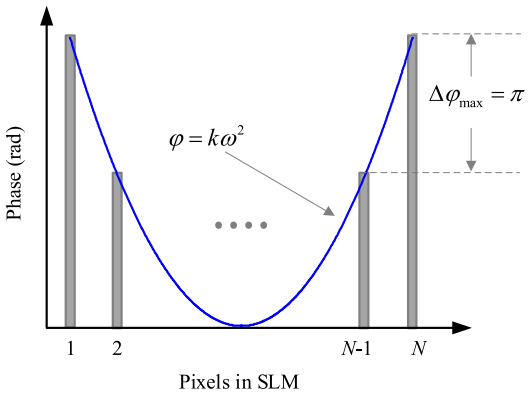

FIGURE 11. **Parabolic phase response recorded in an SLM with a maximum phase coefficient *k*.**

Now we discuss the maximum achievable TBWP of this approach. Similarly, if the optical bandwidth of the spectral shaper is Δf_{opt}, the maximum time duration of the generated pulses is $\tau_{\text{RF}} = 2\pi\Delta f_{\text{opt}}|\ddot{\Phi}|$. As can be seen from Eq. (21), the bandwidth of the chirped microwave waveform is given by $\Delta f_{\text{rf}} = k\tau_{\text{rf}}/(\pi|\ddot{\Phi}|^2)$, which is upper bounded by the maximum phase modulation coefficient. When the phase function recorded in an SLM is parabolic, and the maximum phase jump between neighboring pixels is π in order to avoid phase ambiguity, as shown in Fig. 11, we have the maximum phase modulation coefficient:

$$k_{\max} = \frac{N}{4\pi\Delta f_{\text{opt}}{}^2}. \tag{22}$$

Therefore, the maximum bandwidth of the generated chirped microwave waveform is

$$\Delta f_{\text{rf}} = \frac{k_{\max}\tau_{\text{rf}}}{\pi|\ddot{\Phi}|^2} = \frac{N}{2\pi|\ddot{\Phi}|\Delta f_{\text{opt}}} \tag{23}$$

The maximum achievable TBWP is

$$\text{TBWP}_{\max} = \Delta f_{\text{rf}} \cdot \tau_{\text{rf}} = \frac{N \times 2\pi\Delta f_{\text{opt}}\left|\ddot{\Phi}\right|}{2\pi|\ddot{\Phi}|\Delta f_{\text{opt}}} = N \tag{24}$$

It is seen that the maximum TBWP that can be achieved using a phase-only spectral shaper is equal to the pixel number of the SLM. However, to ensure a high-fidelity output waveform, the phase change between adjacent pixels should be small enough such that the staircase phase pattern in the SLM is a sufficiently good approximation to the desired phase function [53]. If we decrease the maximum phase jump $\Delta\varphi_{\max}$ when setting the phase pattern, the maximum TBWP will decrease accordingly. For example, if $\Delta\varphi_{\max} = \pi/4$, the maximum TBWP is reduced to $N/4$. Another approach to estimate the maximum TBWP is to use the parameter of the maximum group delay (i.e., the dispersion bandwidth product) $\tau_{\text{ss}} = 2\pi|\ddot{\Phi}|\Delta f_{\text{opt}}$ of an SLM-based spectral shaper. Similar to the case of the LCFBG-based approach, the maximum TBWP is given by

$$\text{TBWP}_{\max} = 2\pi\Delta f_{\text{opt}}{}^2\left|\ddot{\Phi}\right| = \tau_{\text{ss}}\Delta f_{\text{opt}}. \tag{25}$$

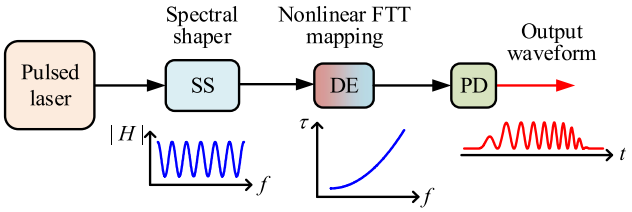

FIGURE 12. **Generation of a chirped microwave waveform based on uniform spectral shaping and nonlinear FTT mapping (using a nonlinear group delay dispersive element).**

It means that the achievable TBWP is upper bounded by the TBWP of the employed spectral shaper. For example, the maximum group delay and the bandwidth of a commercially available spectral shaper (Finisar Waveshaper 4000S) are $\tau_{\text{ss}} = 80$ ps and $\Delta f_{\text{opt}} = 5$ THz [54], respectively, the maximum TBWP is calculated to be 400.

Note that it is different from the maximum TBWP estimation for the scheme based on an amplitude-only spectral shaper, here we calculate the TBWP using the real bandwidth of a microwave waveform with a center frequency of $\delta t/|\ddot{\Phi}|$ according to Eq. (21), but not the maximum frequency. Therefore, if one aims to generate a chirped microwave waveform using a phase-only spectral shaper, the potential of the SLM within the spectral shaper can be fully exploited [29], which mainly owes to the interferometry structure employed in the system.

D. DISCUSSIONS

The approaches discussed are all based on spectral shaping (to obtain a shaped spectrum with a linearly increasing or decreasing FSR) followed by a DE with a linear group delay to implement linear FTT mapping. For chirped microwave waveform generation, we can also use a spectral shaper with a response having a constant FSR (termed uniform spectral shaping), followed by a DE with nonlinear group delay to implement nonlinear FTT mapping [45]–[48]. A system based on nonlinear FTT mapping is shown in Fig. 12. For example, a DE with a first-order dispersion $\ddot{\Phi}$ and a second-order dispersion $\dddot{\Phi}$ (defined as $\dddot{\Phi} = \text{d}\ddot{\Phi}/\text{d}\omega$) can be used to realize nonlinear FTT mapping, given by $\ddot{\Phi}\omega + (1/2)\dddot{\Phi}\,\omega^2 \Leftrightarrow t$ [45]–[48]. It has been demonstrated that an optical fiber with a higher order dispersion can be used to implement nonlinear FTT mapping to generate a chirped microwave waveform [45]. However, due to the limited second-order dispersion of a standard single mode fiber, the experimentally generated chirped microwave waveforms have a low chirp rate and small TBWP. To increase the chirp rate and TBWP, specially designed nonlinearly chirped FBGs with large second-order dispersion can be used [46], [48]. The fabrication can be performed by using a nonlinearly chirped phase mask [55] or a linearly chirped phase mask, but with the second-order dispersion introduced via controlling the exposure pattern during the fabrication [56]. A nonlinearly chirped FBG can also be produced from a linearly chirped FBG based on strain-gradient

TABLE 1. TBWPs of the Approaches for Chirped Microwave Waveform Generation Based on SS-FTT Mapping

Method		Theoretical $TBWP_{max}$ *	TBWP realized experimentally
Spectral shaper with LCFBG(s)	MZI with LCFBG(s)	$2\pi\Delta f^2\lvert\ddot{\Phi}\rvert$ or $4\pi\Delta f^2\lvert\ddot{\Phi}\rvert$ **	45.56 [21]
	Super-imposed LCFBGs	$4\pi\Delta f^2\lvert\ddot{\Phi}\rvert$	37.5 [18]
	Sagnac loop with LCFBG	$4\pi\Delta f^2\lvert\ddot{\Phi}\rvert$	44.8 [19]
Spectral shaper using a dispersive fiber	MZI with a dispersive fiber	$2\pi\Delta f^2\lvert\ddot{\Phi}\rvert$	527 [23]
Programmable spectral shaper with an SLM	Amplitude-only SLM	$N/2$	61.2 [27]
	Phase-only SLM in an MZI	N ***	589 [29]
Spectral shaper based on a PIC	PIC (LCWBGs in an MZI)	$4\pi\Delta f^2\lvert\ddot{\Phi}\rvert$	615 [43]
	PIC (CWBGs in a Sagnac loop)	$4\pi\Delta f^2\lvert\ddot{\Phi}\rvert$	15-20 [42]
	PIC (Super-imposed LCWBGs) DFPC	$4\pi\Delta f^2\lvert\ddot{\Phi}\rvert$	14.5 [41]
Sinusoidal spectral shaping + Nonlinear FTT mapping		$2\pi\Delta f^2 t_0\lvert\ddot{\Phi}\rvert/\lvert\ddot{\Phi}\rvert$	5.45 [47]

* If two LCFBGs are employed, they are assumed to be identical but oppositely oriented and have an absolute dispersion value of $|\ddot{\Phi}|$.
**Depending on the employment of one LCFBG or two LCFBGs with opposite dispersion.
***This $TBWP_{max}$ is estimated by assuming the maximum phase jump between adjacent pixels is π. If the maximum phase jump decreases, the value of $TBWP_{max}$ will decrease proportionally.

beam tuning. The use of such an FBG to generate a linearly chirped microwave waveform has been demonstrated [47].

An optical filter with a sinusoidal spectral response can be realized based on a two-tap delay line structure with a time delay difference of δt. After spectral shaping and nonlinear FTT mapping, a linearly chirped microwave waveform is generated. The instantaneous frequency of the generated chirped microwave waveform is given by [45]

$$\omega(t) \approx \frac{\delta t}{|\ddot{\Phi}|} - \frac{\dddot{\Phi}\,\delta t}{|\ddot{\Phi}|^2}t. \tag{26}$$

The time duration of the waveform is as

$$\tau_{\mathrm{rf}} = |2\pi\,\Delta f_{\mathrm{opt}}\dddot{\Phi} + 2\pi^2\Delta f_{\mathrm{opt}}{}^2\ddot{\Phi}\,|. \tag{27}$$

The bandwidth of the generated chirped microwave waveform is estimated to be

$$\Delta f_{\mathrm{rf}} = \frac{1}{2\pi}\frac{|\dddot{\Phi}\,|\delta t}{|\ddot{\Phi}|^2}\tau_{\mathrm{rf}}. \tag{28}$$

Therefore, the TBWP can be calculated based on Eqs. (27) and (28).

Table I summarizes the theoretical and experimental TBWP values for the approaches based on SS-FTT mapping. In most cases, the experimentally achieved TBWP values are lower than the theoretical maximum ones, since the TBWP values achieved in the experiments depend on the actual parameters, such as the overall bandwidth of the systems and dispersion values of the DEs and/or Bragg gratings.

III. CHIRPED MICROWAVE WAVEFORM GENERATION BASED ON FREQUENCY MULTIPLICATION

A. FREQUENCY MULTIPLICATION USING MZM(S) [57]–[65]

Photonic generation of microwave signals based on external modulation has been well studied [57]–[61]. Through frequency multiplication, a high-frequency microwave signal can be generated from a low-frequency reference signal with the frequency multiplication implemented using an MZM or a phase modulator. In [58], a continuously tunable microwave signal with a quadrupled frequency using an MZM that is biased at the maximum transmission point was generated. In [59], a phase modulator was employed to realize frequency doubling. The advantage of using a phase modulator is that no bias is needed, thus no sophisticated bias control is required. A similar approach based on a dual parallel polarization modulator (DP-PolM) was reported, in which a frequency-doubled microwave signal was generated [61].

The methods reported in [58], [59] can also been employed to generate a chirped microwave waveform by using a low-frequency and small-bandwidth chirped microwave waveform as a reference signal, in which both the center frequency and the bandwidth are multiplied, thus leading to a multiplied TBWP.

In [61], an MZM-based approach to generating a frequency- and bandwidth-doubled chirped microwave waveform was reported. Thanks to the increased TBWP, the waveform was used in a microwave photonic inverse synthetic aperture radar to improve the imaging resolution. The schematic of the approach is illustrated in Fig. 13, where an MZM biased at the null point is employed.

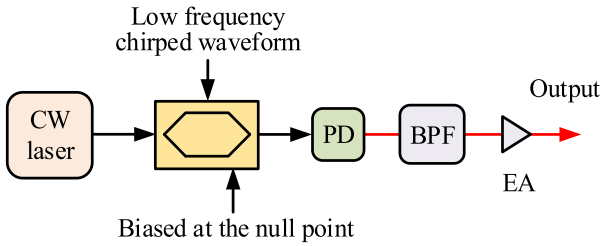

FIGURE 13. Generation of a chirped microwave waveform with frequency doubling using an MZM (PD: photodetector; MZM: Mach-Zehnder modulator; BPF: bandpass filter; EA: electronic amplifier).

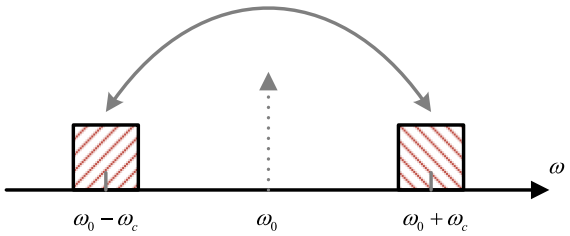

FIGURE 14. Optical spectrum of a modulated chirped microwave waveform, where the optical carrier is suppressed, ω_0 and ω_c are the frequency of the optical carrier and the center frequency of the microwave waveform, respectively.

A low-frequency chirped microwave waveform is generated electronically which is used as a reference,

$$S_{in}(t) = V_{in} rect\left(\frac{t}{T_p}\right)\cos\left(\omega_c t + k\pi t^2\right) \tag{29}$$

where V_{in}, ω_c, and $k = B/T_p$ are the amplitude, center frequency and chirp rate of the reference chirped waveform, respectively (where B and T_p are the bandwidth and duration, respectively), $rect(t/T_p)$ is a rectangular function with a width of T_p. After modulation at the MZM, the complex envelope of the modulated waveform is given by

$$E(t) = \frac{\sqrt{P_0}}{2}\left\{\exp\left[j(\varphi_s(t) + \varphi_b)\right] + \exp\left[-j\varphi_s(t)\right]\right\} \tag{30}$$

where P_0 is the optical power from the laser source, $\varphi_s(t)$ is the phase shift due to phase modulation given by $\varphi_s(t) = S_{in}(t)/V_\pi$, where V_π is the half-wave voltage of the MZM, $\varphi_b = V_b/V_\pi$ is the bias-induced phase shift due to the bias voltage V_b. Here it is assumed that a push-pull MZM is employed. To achieve frequency doubling, the bias voltage should be controlled to introduce a phase shift $\varphi_b = \pi$. In this case, the optical carrier is fully suppressed. The optical spectrum of the optical signal at the output of the MZM is shown in Fig. 14. After square-law detection, the photo-current at the output of the PD is a result of the heterodyne beating between the upper- and lower sidebands, which is given by

$$I_{out}(t) = I_0 rect(t/T_p)\cos(2\omega_c t + 2k\pi t^2) \tag{31}$$

where I_0 is the amplitude of the output waveform, which is determined by the optical power and the responsivity of the PD. It is seen that the carrier frequency and bandwidth of the generated microwave waveform are both doubled. Note that there are always power loss and noise increase in the multiplication process, which inevitably lead to an increase in noise figure. The use of an MZM with a lower half-wave voltage and a PD with higher power handling capability would reduce the noise figure.

A frequency- and bandwidth-quadrupled chirped microwave waveform can be generated using a dual-parallel MZM. Again, since the generated waveform has a quadrupled bandwidth, the generated chirped waveform was employed in an inverse synthetic aperture radar to improve the imaging resolution [62].

To improve the range-Doppler resolution in a radar system, a dual-chirp microwave waveform can be used. A dual-chirp signal consists of two overlapping chirped microwave waveforms with opposite frequency chirping, one up-chirped and the other down-chirped. The idea of transmitting a dual-chirped microwave waveform was proposed to overcome the range-Doppler coupling effect [65]. Again, through external modulation, a dual-chirp microwave waveform with both increased carrier frequency and bandwidth can be generated [63]–[64]. For example, in [63], a baseband chirped microwave waveform is upconverted to a higher frequency using a dual-parallel MZM. The use of two cascaded MZMs can also generate a dual-chirp microwave waveform with both the carrier frequency and bandwidth quadrupled [64].

B. FREQUENCY MULTIPLICATION BASED ON PHOTONIC TIME COMPRESSION [66]–[73]

Photonic time stretch (PTS) is a technique to slow down an ultrafast signal prior to its digitization by an electronic analog-to-digital converter [66]–[67]. In a PTS system, an ultrashort optical pulse generated by a pulsed laser is sent to a DE, where the pulse is time-stretched and frequency-chirped, which is sent to an MZM at which an analog microwave signal is modulated on the chirped pulse. The modulated chirped pulse is then sent to a second DE (with the same sign of dispersion as the first one), which makes the pulse further time stretched. Photodetection of this further-stretched pulse would generate a new analog microwave signal which is a time-stretched replica of the input analog microwave signal. The technique of PTS has shown great potential for ultra-wideband data acquisition, imaging, and real-time measurement of rare events. A PTS-assisted real-time digitizer with an equivalent sampling rate as high as a tera-sample per second has been demonstrated [67].

On the other hand, photonic time compression (PTC) can be implemented based on the same concept. If the second DE in a PTS system has an opposite dispersion, the system can perform time compression or time reversal of a microwave waveform [68].

Fig. 15 shows a PTC system for frequency upconversion [69]–[73]. As can be seen, two DEs with dispersion values of $\ddot{\Phi}_1$ and $\ddot{\Phi}_2$ are placed before and after an MZM. To achieve time compression, $\ddot{\Phi}_1$ and $\ddot{\Phi}_2$ should be selected such that $\mathrm{sgn}(\ddot{\Phi}_2) = -\mathrm{sgn}(\ddot{\Phi}_1)$ and $|\ddot{\Phi}_2| < |\ddot{\Phi}_1|$. An ultra-short optical pulse from a pulsed laser is dispersed by the first DE, which

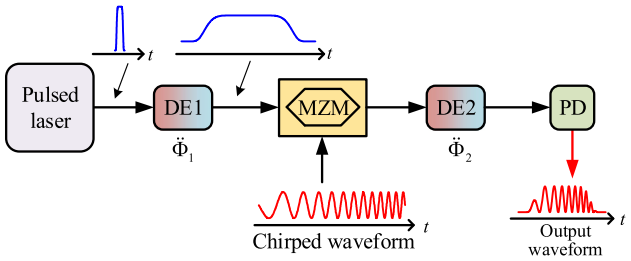

FIGURE 15. Frequency and bandwidth multiplication based on photonic time compression with a dispersion configuration of $\mathrm{sgn}(\ddot{\Phi}_2) = -\mathrm{sgn}(\ddot{\Phi}_1)$ and $|\ddot{\Phi}_2| < |\ddot{\Phi}_1|$ (DE: dispersive element; MZM: Mach-Zehnder modulator; PD: photodetector).

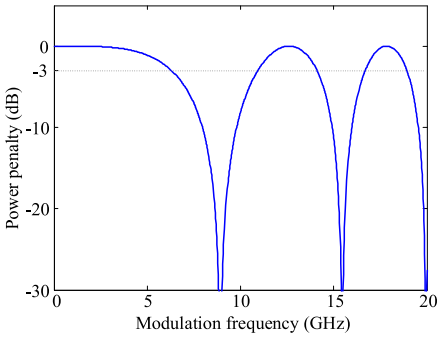

FIGURE 16. A typical frequency-dependent microwave power fading function induced by the double-sideband modulation and chromatic dispersion in a photonic time compression system ($\ddot{\Phi}_2 = 200$ ps^2 and $M = 1/5$).

is then modulated by a microwave waveform within the time window of the dispersed pulse at the MZM. The modulated chirped pulse is then sent to a second DE where the pulse is compressed due to the opposite dispersion, which leads to frequency upconversion of the input microwave waveform [69]–[73]. The pulse compression ratio, or the frequency multiplication factor, is determined by the dispersion values of the two DEs.

It should be noted that a PTC system can also be viewed as an unbalanced temporal pulse shaping (TPS) systems, which has been well studied [70]–[71]. A PTC system can be analyzed based on the temporal Talbot effect [72]. Due to the frequency-dependent phase shift between the upper and lower modulation sidebands caused by chromatic dispersion, there is a frequency-dependent microwave power fading, similar to the well-known dispersion-induced power penalty in a radio over fiber system. At some modulation frequencies, the output microwave power would vanish since the beating between the optical carrier with the upper sideband will cancel completely the beating between the optical carrier with the lower sideband at the PD. Assume a push-pull MZM biased at the quadrature point is employed, the frequency-dependent microwave power fading (or frequency response) can be expressed as

$$|H(\omega RF)|^2 = \cos^2\left(\frac{\ddot{\Phi}_2 {\omega_{RF}}^2}{2M}\right), \tag{32}$$

where $M = (\ddot{\Phi}_1 + \ddot{\Phi}_2)/\ddot{\Phi}_1$ is the compression factor ($M < 1$) and ω_{RF} is the modulation frequency. A typical frequency-dependent microwave power fading function is plotted in Fig. 16, where $\ddot{\Phi}_2 = 200$ ps^2 and $M = 1/5$ are assumed.

Note that the process of time stretch or compression does not change the TBWP of a generated microwave waveform, as the bandwidth of the output waveform is inversely proportional to its temporal duration. The upper limit of the TBWP of a PTC system depends on the bandwidth (frequency response) and the time aperture of the optical pulse after the first DE. According to Eq. (32) and Fig. 16, the 3-dB bandwidth of the PTC system is equal to $\Delta f_{\mathrm{rf}} = [M/(8\pi|\ddot{\Phi}_2|)]^{1/2}$. The time aperture of the system is given by $\tau_{\mathrm{rf}} = 2\pi\Delta f_{\mathrm{opt}}|\ddot{\Phi}_1|$, where Δf_{opt} is the optical bandwidth of the short pulse. The TBWP of the PTC system is thus given by

$$\mathrm{TBWP} = \tau_{\mathrm{rf}}\Delta f_{\mathrm{rf}} = \left|\frac{\pi M\ddot{\Phi}_1}{2(1-M)}\right|^{1/2} \cdot \Delta f_{\mathrm{opt}}. \tag{33}$$

It is seen from Eq. (33) that for a given compression factor (or the dispersion values of the two DEs), the TBWP of a PTC system increases with the increase in the optical bandwidth of the short pulse.

It should be noted that a passband microwave waveform (the lowest frequency does not start from DC) can also be compressed, but the spectrum of the input microwave waveform should fall in one of the multiple passbands of the frequency response, shown in Fig. 16 [74].

For an input optical pulse with a sufficiently wide spectral width, the achievable TBWP is also limited by the microwave power fading function induced by the use of optical double sideband with carrier (DSB+C) modulation. There are some techniques to improve the TBWP. The first one is to employ a single-arm MZM with chirp biased at the quadrature point instead of a chirp-free push-pull MZM. In this case, the power fading function is modified to be $|H(\omega RF)|^2 = \cos^2(\frac{\ddot{\Phi}_2{\omega_{RF}}^2}{2M} \pm \frac{\pi}{4})$. It is found that the baseband bandwidth and therefore the TBWP can be improved by around 40%. The second approach is to employ optical single sideband with carrier (SSB+C) modulation to eliminate the microwave power fading. Optical SSB+C modulation can be realized by filtering out one of optical sidebands or using a dual-port MZM with the help of a 90° hybrid coupler. However, both schemes are not easy to realize, especially over a wide microwave bandwidth. A third approach is to exploit the phase diversity between the two modulated signals at the outputs of a dual-output MZM. It was demonstrated that the power fading problem can be fully eliminated by combining the two complementary outputs [75].

IV. CHIRPED MICROWAVE WAVEFORM GENERATION BASED ON FOURIER-DOMAIN MODE LOCKING

An OEO can be used to generate a low phase noise microwave signal due to the high Q factor of the OEO loop [76]–[79]. A

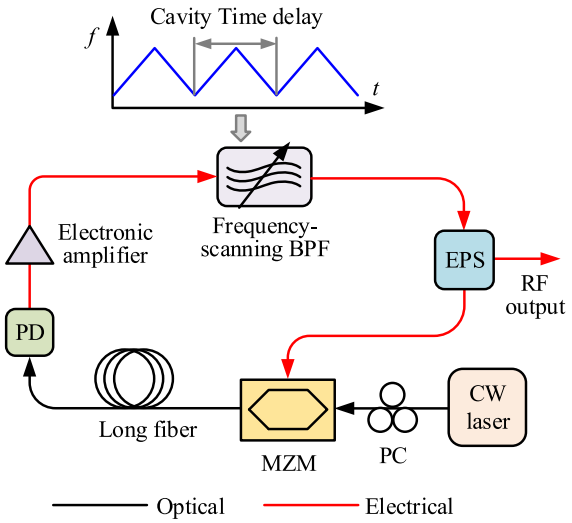

FIGURE 17. **A Fourier domain mode locked OEO for generating a chirped microwave waveform (EPS: electronic power splitter; MZM: Mach-Zehnder modulator; PC: polarization controller).**

chirped microwave waveform can also be generated by a fast frequency tunable OEO, but the phase noise performance is poor due to the fact that the OEO, when being tuned from one frequency to another, will need a buildup time to stabilize the oscillation at the new frequency [80]. A solution is to use Fourier domain mode locking. In a Fourier domain mode locked (FDML) OEO, all modes are phase locked and co-exist in the OEO loop; the switching from one mode to another mode will not need a buildup time; thus a chirped microwave waveform generated by an FDML OEO will have a low phase noise [81]–[85].

Fig. 17 shows the schematic of an FDML OEO, which has a hybrid cavity consisting of an optical path and electric paths. A section of long fiber forms the optical path. In the electrical path, there are an electronic amplifier (EA) and a frequency-rapidly-scanning narrow bandpass filter (BPF) (a dynamic filter). According to the theory of Fourier domain mode locking, as long as the dynamic filter repeats its spectrogram with a period equal to the round-trip time of the cavity, Fourier domain mode locking is achieved, and a frequency-scanning (chirped) microwave waveform is generated.

The key component in an FDML OEO is the electronic fast frequency-scanning BPF, which is hard to implement electronically, especially considering the large tunable range and fast tuning speed. A solution is to implement the frequency scanning BPF based on microwave photonic technique [82]. Fig. 18 shows a microwave photonic frequency-scanning bandpass filter. The filter is realized based on phase modulation and phase modulation to intensity modulation conversion, to translate the notch of an optical filter to the passband of the BPF. As can be seen, a light wave from a tunable laser source (TLS) is sent to a phase modulator to which a microwave signal is applied. A phase modulated signal with two sideband and an optical carrier is generated at the output the phase modulator. An optical notch filter, which can be a phase-shifted

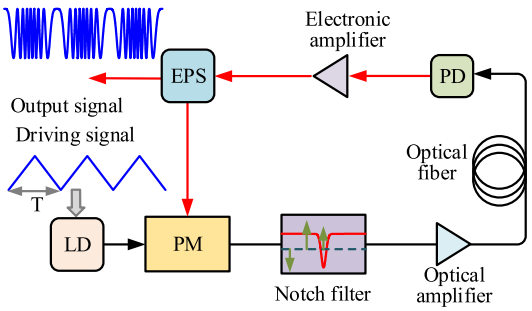

FIGURE 18. **Fourier-domain mode-locked OEO with a fast tuning microwave photonic bandpass filter (EPS: electronic power splitter; LD: laser diode; PD: photodetector; PM: phase modulator).**

FBG operating in the reflection mode, is employed to remove one of the two sidebands. Due to the removal of a sideband of the phase-modulated signal, phase modulation is converted to intensity modulation and the overall operation is equivalent to a BPF with the center frequency of the passband being determined by the frequency difference between frequency of the optical carrier and the center frequency of the optical notch filter. To achieve frequency tuning, the TLS is operating in a wavelength sweeping mode realized by injecting a sawtooth driving current to the laser diode in the TLS. It was experimentally demonstrated that an FDML OEO can generate a chirped microwave waveform with a bandwidth of 7.5 GHz and a scanning rate of 0.34 GHz/μs. Thanks to the long-time duration of the generated chirped microwave waveform, the TBWP is very large. For the demonstration reported in [82], the TBWP was estimated as large as 1.6×10^5. The phase noise of the generated signal is also very low, which is -134.5 dBc/Hz at 10 kHz offset.

More recently, an FDML OEO with the frequency-scanning BPF implemented based on stimulated Brillouin scattering (SBS) was reported [84]–[85]. The advantage of using the SBS effect to implement a frequency-scanning BPF is the narrow bandwidth of the SBS gain or loss spectrum, which makes the BPF have a narrow bandwidth, which is highly needed for accurate mode selection in achieving Fourier domain mode locking. The reported TBWP values achieved in the experiments in [84] and [85] are 23850 and 22446, respectively.

The work on FDML OEO for chirped microwave waveform generation has shown its great potential in generating high quality and large TBWP chirped microwave waveforms which are highly needed in high resolution imaging systems and wideband microwave photonic signal processing systems.

One key challenge in implementing a frequency-scanning BPF based on microwave photonics is the complicated structure and low energy efficiency due to OE and EO conversions involved. Recently, an FDML OEO using a diode-tuned bandpass filter was reported, which features a simplified system and low power consumption [86].

V. INTEGRATED ON-CHIP SPECTRAL SHAPER [33]–[44]

In recent years, on-chip microwave photonic signal processing and generation using PICs have attracted great attention due to

the advantages of much smaller size, better stability and reliability, and lower power consumption of PICs. In addition, the CMOS-compatible fabrication process makes PICs have high potential for mass production at low cost. Silicon-based PICs have been proposed and demonstrated for arbitrary microwave waveform generation including the generation of chirped microwave waveforms. Most of the work is based on SS-FTT mapping. In this Section, photonic integrated solutions for chirped microwave waveform generation based on SS-FTT mapping will be discussed [35]–[44].

A spectral shaper can be implemented based on silicon photonic microring resonators [36]–[38]. The advantage of using a microring resonator based spectral shaper is that reconfigurable ultrabroad-band microwave waveforms can be generated with cycle-by-cycle frequency control through thermal tuning of the individual microring resonators in the spectral shaper. The major limitation of this approach is that the overall temporal duration of the generated microwave waveforms is limited due to the small number of cycles in the generated microwave waveforms which is equal to the number of the microring resonators used. With the advancement in silicon photonics, a large number of microring resonators on a single chip can now be implemented, which is able to provide a large number of cycles, leading to a microwave waveform with a much longer temporal duration [39], [40].

A spectral shaper can also be implemented based on two superimposed silicon photonic chirped Bragg gratings, to form a distributed Fabry-Perot cavity (DFPC) [41] (an integrated version of the scheme shown in Fig. 4). The principle in terms of chirped microwave waveform generation is identical to that reported in [18]. As shown in Fig. 4, two photonic integrated chirped Bragg gratings with opposite dispersion are separated spatially by an offset to form a DFPC. It is different from a fiber-based chirped Bragg grating in which the chirp is produced by changing the period of the grating, a silicon photonic Bragg grating is usually fabricated based on sidewall corrugations with identical period, but with the chirp produced by increasing or decreasing width along the grating structure, to change the effective refractive index along the grating. In the demonstration reported in [41], for the two Bragg gratings with a length of 157.5 μm and a chirp rate of 12.2 nm/mm, a chirped microwave waveform with a TBWP of 14.5 was generated.

By incorporating a chirped waveguide Bragg grating in a Sagnac loop (an integrated version of the scheme shown in Fig. 5), a spectral shaper with an increasing or decreasing FSR can be implemented [42]. By using the spectral shaper, a chirped microwave waveform can be generated based on FTT mapping. In the demonstration reported in [42], for a chirped Bragg grating with a length of 3.2 mm and a chirp rate of 0.26 nm/mm, a chirped microwave waveform with a TBWP of around 15 was generated.

According to Eq. (11), the upper limit of the TBWP is limited by the bandwidth and group delay (product of the length and chirp rate) of the grating(s) within a PIC. Therefore, the key to increase the TBWP is to increase the length and bandwidth of the grating(s). Zhang and Yao proposed and demonstrated a silicon photonic spectral shaper with two chirped gratings on a silicon chip having an increased length and bandwidth [43]. The principle of the spectral shaper is the same as that reported in [16], shown in Fig. 19 with the perspective view of a chirped grating shown in Fig. 20. The length of a fabricated waveguide grating can be as long as 12.54 mm and the measured group delay and bandwidth can be as high as 241 ps and 29 nm (1533-1562 nm or 3633 GHz), respectively, corresponding to a maximum TBWP of around 1751 according to Eq. (11). In the experimental demonstration reported in [43], for two waveguide gratings with a group delay of 228 ps and a bandwidth of 11 nm, a chirped microwave waveform with a TBWP of 615 was generated ($\text{TBWP}_{\text{max}} \approx 635$ in theory).

An on-chip spectral shaper with tuning ability based on silicon photonics was also demonstrated [44]. In this work, spectral shaper based on a Michelson interferometer structure with two tunable waveguide gratings in its two arms was implemented. By introducing a lateral PN junction to each of the two gratings, thanks to the plasma dispersion effect, the chirp rate of each of the gratings can be independently tuned by changing the injection current to the PN junction. The tuning speed is ultra-high, which is in the order of nanoseconds. In the implementation [44], the DE to perform FTT mapping was

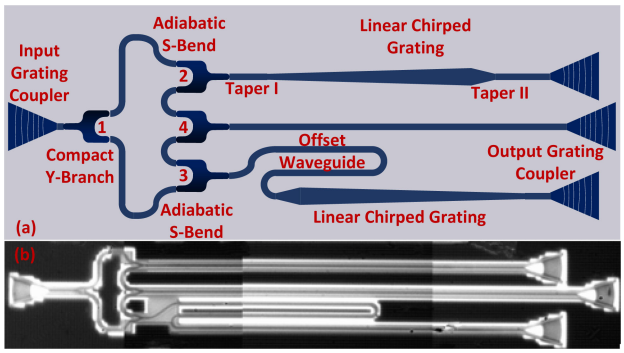

FIGURE 19. (a) An on-chip spectral shaper based on two chirped gratings; (b) Image of the fabricated spectral shaper captured by a microscope camera.

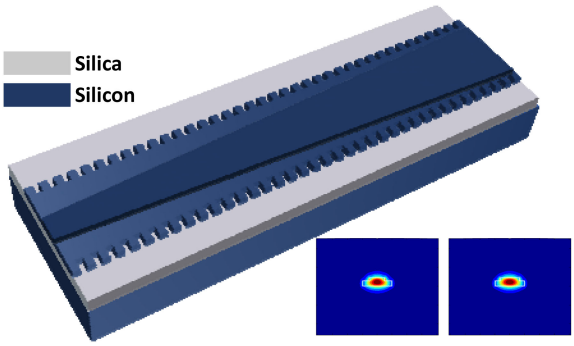

FIGURE 20. Perspective view of an integrated chirped grating. Inset: Simulated fundamental TE mode profile of the rib waveguide with the rib width of 500 nm (left) and 650 nm (right).

a length of dispersion compensating fiber (DCF) with a group velocity dispersion (GVD) of –1020 ps/nm. An integrated chirped waveguide grating can be used as a dispersive delay line, but the dispersion value is very limited (around 20 ps/nm) due to the small length of an integrated chirped waveguide grating [43], [44]. Solutions must be found to implement a dispersive delay line with a large dispersion on an integrated platform.

Chirped microwave waveform generation based on frequency multiplication, shown in Fig. 13 [61], can be implemented on an integrated platform. For example, the MZM and the PD can both be implemented on a silicon platform [33], [34]. Since silicon is not a direct bandgap material, no light can be generated. The laser source has to be implemented based on a direct bandgap material, such as InP. Thus, either an external light source is used to couple light into the chip, but the system is not monolithically integrated, or heterogenous integration is implemented, although a challenging process, but it can make the system on a single chip.

An FDML OEO can be used to generate a chirped microwave waveform with a large TBWP. The implementations reported were based on pure fiber optics [83] or partially photonic integrated [90]. It is very challenging to implement an FDML OEO based on a fully photonic integrated circuit. The long loop length of a few to tens of meters to ensure a large number of longitudinal modes in the laser cavity makes it extremely hard to implement an FDML OEO in a single chip due to the small diremptions of a PIC.

More details about silicon photonics for wideband microwave waveform generation and their applications can be found in [14], [33], [34].

VI. DISCUSSIONS AND SUMMARY

Apart from the above discussed methods, chirped microwave waveforms can also be generated based on heterodyne beating between a continuous-wave (CW) light wave at a fixed wavelength and a wavelength-sweeping light wave from a wavelength-swept laser source [87]–[92]. It was demonstrated in [87] that a chirped microwave waveform with a spectral width covering 89-103 GHz with a sweeping time of 50 μs was generated. The TBWP is as large as 7×10^5. In addition, a linearly chirped microwave waveform can be generated based on heterodyne beating between a CW light wave and a pre-chirped optical pulse [89]. Recently, a hybrid FDML laser was proposed for the generation of a wideband linearly chirped microwave waveform [90]. The frequency-scanning BPF was implemented using a silicon photonic integrated micro disk, which has narrow bandwidth and can operate at a fast-tuning speed. The microwave waveform was generated based on heterodyne beating between a CW light wave and a wavelength-sweeping light wave from the hybrid FDML laser. It was demonstrated that the bandwidth and time width of the generated chirped microwave waveforms can be over 50 GHz and 30 μs, respectively. The achieved TBWP is over 1.5×10^6.

In addition, a microwave photonic transversal filter with a nonlinear phase response can be used to convert a broadband chirp-free microwave pulse to a chirped microwave waveform. The operation is identical to a PTS system, but in the microwave domain. With this method, a linearly chirped microwave waveform with a chirp rate of 13.2 MHz/ps by using a five-tap microwave photonic filter was demonstrated [91]. The bandwidth is small due to a small number of taps used in the microwave photonic transversal filter. To increase the bandwidth, a transversal filter with a greater number of taps is needed. The use of an optical comb with a large number of comb lines can be used to implement a transversal filter with a large number of taps [93].

In summary, we have reviewed the recent advances in the generation of wideband chirped microwave waveforms based on microwave photonics. Three major methods have been discussed, including chirped microwave generation based on SS-FTT mapping, frequency and bandwidth multiplication, and Fourier domain mode locking of an OEO. In particular, we studied the maximum TBWP that can be achieved for each of the methods. Among the three methods, the one based on SS-FTT mapping has been extensively studied and a large number of papers have been published. The limitation of this method is that the temporal width of a generated chirped microwave waveform is narrow, thus the TBWP is small. The use of LCFBGs in a spectral shaper with much longer length can increase the TBWP. For example, an LCFBG with an overall length of a few meters is now available [95]. The use of such LCFBGs can increase significantly the TBWP. The implementation of such a long LCFBG on an integrated chip is still challenging. The method using frequency multiplication based on external modulation can generate a chirped microwave waveform with a much greater TBWP. It also provides a solution that is more feasible for practical applications thanks to the simplicity and stability. Generation systems based on the second method have been employed in microwave photonic radars [61], [62]. The method based on an FDML OEO has the key advantages of very large TBWP and low phase noise. It is the most promising method for high-quality and large-TBWP chirped microwave waveform generation.

Note that the sampling rate of electronic AWGs has been increasing greatly and a state-of-the-art AWG can have a sampling rate higher than 100 GSa/s. On the other hand, the bandwidth of a photonic-based microwave waveform generation system is mainly limited by the bandwidth of the PDs. Currently, commercially available PDs with a bandwidth over 300 GHz are available. Therefore, photonic approaches for the generation of wideband microwave waveforms are still being actively researched due to the huge bandwidth potential.

Despite tremendous progress has been made over the last 30 years, there are still challenges that limit the techniques for wider applications [94]. The first challenge is how to flexibly control the bandwidth and time duration of a generated microwave waveform. The second challenge is how to improve the performance of the generated signals, especially the phase noise performance, since it has major impact on a

high-performance radar or an imaging system. Finally, the size of most of the systems is large, which also limits the techniques for practical applications. A solution is to implement a system on a PIC in which hybrid integration of light sources, optical amplifiers, all other passive and active photonic components, and analog and digital electronics is implemented. This is in fact a highly challenging task, but it is the future of microwave photonics.

REFERENCES

[1] M. I. Skolnik, *Introduction to Radar Systems*, 2nd ed. Singapore: McGraw-Hill, 1980.

[2] M. I. Skolnik, "Role of radar in microwaves," *IEEE Trans. Microw. Theory Techn.*, vol. 50, no. 3, pp. 625–632, Mar. 2002.

[3] A. W. Rihaczek, *Principles of High-Resolution Radar*. Norwood, MA, USA: Artech House, 1996.

[4] A. S. Mudukutore, V. Chandrasekar, and R. J. Keeler, "Pulse compression for weather radars," *IEEE Trans. Geosci. Remote Sens.*, vol. 36, pp. 125–142, Jan. 1998.

[5] H. Kwon and B. Kang, "Linear frequency modulation of voltage controlled oscillator using delay-line feedback," *IEEE Microw. Wireless Compon. Lett.*, vol. 15, no. 6, pp. 431–433, Jun. 2005.

[6] H. D. Griffiths and W. J. Bradford, "Digital generation of high time bandwidth product linear FM waveforms for radar altimeters," *Proc. Inst. Elect. Eng. F, Radar Signal Process.*, vol. 139, no. 2, pp. 160–169, Apr. 1992.

[7] A. M. Kawalec, "SAW dispersive delay lines in radar signal processing," in *Proc. IEEE Int. Radar Conf.*, 1995, pp. 732–736.

[8] D. K. Barton, *Radar System Analysis and Modeling*. Boston, MA, USA: Artech House, 2005.

[9] J. Capmany and D. Novak, "Microwave photonics combines two worlds," *Nature Photon.,* vol. 1, pp. 319–330, Jun. 2007.

[10] J. Yao, "Microwave photonics," *J. Lightw. Technol.*, vol. 27, no. 3, pp. 314–335, Feb. 2009.

[11] J. Yao, "Photonic generation of microwave arbitrary waveforms," *Opt. Commun.*, vol. 284, no. 15, pp. 3723–3736, Jul. 2011.

[12] R. Minasian, E. W. H. Chan, and X. Yi, "Microwave photonic signal processing," *Opt. Exp.*, vol. 21, no. 19, pp. 22918–22936, Sep. 2013.

[13] J. Capmany, J. Mora, I. Gasulla, J. Sancho, J. Lloret, and S. Sales, "Microwave photonic signal processing," *J. Lightw. Technol.*, vol. 31, no. 4, pp. 571–586, Feb. 2013.

[14] L. R. Chen, "Photonic generation of chirped microwave and millimeter wave pulses based on optical spectral shaping and wavelength-to-time mapping in silicon photonics," *Opt. Commun.*, vol. 373, pp. 70–81, Aug. 2016.

[15] A. M. Weiner, "Optical pulse shaping: A tutorial review," *Opt. Commun.*, vol. 284, no. 15, pp. 3669–3692, Jul. 2011.

[16] A. Zeitouny, S. Stepanov, O. Levinson, and M. Horowitz, "Optical generation of linearly chirped microwave pulses using fiber bragg gratings," *IEEE Photon. Technol. Lett.*, vol. 17, no. 3, pp. 660–662, May 2005.

[17] H. Chi, F. Zeng, and J. Yao, "Photonic generation of microwave signals based on pulse shaping," *IEEE Photon. Technol. Lett.*, vol. 19, no. 5, pp. 668–670, May 2007.

[18] C. Wang and J. Yao, "Photonic generation of chirped microwave pulses using superimposed chirped fiber bragg gratings," *IEEE Photon. Technol. Lett.*, vol. 20, no. 11, pp. 882–884, Mar. 2008.

[19] C. Wang and J. Yao, "Chirped microwave pulse generation based on optical spectral shaping and wavelength-to-time mapping using a sagnac loop mirror incorporating a chirped fiber bragg grating," *J. Lightw. Technol.*, vol. 27, no. 12, pp. 3336–3341, Aug. 2009.

[20] C. Wang and J. Yao, "Large time-bandwidth product microwave arbitrary waveform generation using a spatially discrete chirped fiber bragg grating," *J. Lightw. Technol.*, vol. 28, no. 11, pp. 1652–1660, Jun. 2010.

[21] M. Li and J. Yao, "Photonic generation of continuously tunable chirped microwave waveforms based on a temporal interferometer incorporating an optically-pumped linearly-chirped fiber Bragg grating," *IEEE Trans. Microw. Theory Techn.*, vol. 59, no. 12, pp. 3531–3537, Dec. 2011.

[22] H. Zhang, W. Zou, and J. Chen, "Generation of a widely tunable linearly chirped microwave waveform based on spectral filtering and unbalanced dispersion," *Opt. Lett.*, vol. 40, no. 6, pp. 1085–1088, Mar. 2015.

[23] H. Zhang *et al.*, "Experimental generation of linearly chirped 350 GHz band pulses with a bandwidth beyond 60 GHz," *Opt. Lett.*, vol. 42, no. 24, pp. 5242–5245, Dec. 2017.

[24] A. M. Weiner, "Femtosecond pulse shaping using spatial light modulators," *Rev. Sci. Instruments*, vol. 71, no. 5, pp. 1929–1960, Jan. 2000.

[25] I. S. Lin, J. D. McKinney, and A. M. Weiner, "Photonic synthesis of broadband microwave arbitrary waveforms applicable to ultra-wideband communication," *IEEE Microw. Compon. Lett.*, vol. 15, no. 4, pp. 226–228, Apr. 2005.

[26] J. D. McKinney, D. S. Seo, and A. M. Weiner, "Photonically assisted generation of continuous arbitrary millimeter electromagnetic waveforms," *Electron. Lett.*, vol. 39, no. 3, pp. 309–311, Feb. 2003.

[27] Y. Mei *et al.*, "Photonic generation of chirped microwave signals with high time-bandwidth product," *Opt. Commun.*, vol. 316, pp. 106–110, Apr. 2014.

[28] Y. Mei, T. Jin, H. Chi, S. Zheng, X. Jin, and X. Zhang, "Characterization of the photonic generation of phase-coded RF signals based on pulse shaping and frequency-to-time mapping," *Appl. Opt.*, vol. 54, no. 13, pp. 3956–3962, 2015.

[29] A. Rashidinejad and A. M. Weiner, "Photonic radio-frequency arbitrary waveform generation with maximal time-bandwidth product capability," *J. Lightw. Technol.*, vol. 32, no. 20, pp. 3383–3393, Oct. 2014.

[30] Y. Li, A. Rashidinejad, J.-M. Wun, D. E. Leaird, J.-W. Shi, and A. M. Weiner, "Photonic generation of W-band arbitrary waveforms with high time-bandwidth products enabling 3.9 mm range resolution," *Optica*, vol. 1, no. 6, pp. 446–454, Dec. 2014.

[31] V. Torres-Company, D. E. Leaird and A. M. Weiner, "Dispersion requirements in coherent frequency-to-time mapping," *Opt. Exp.*, vol. 19, no. 24, pp. 24718–24729, Nov. 2011.

[32] Y. Xu, Z. Shi, H. Chi, X. Jin, S. Zheng, and X. Zhang, "Relaxed dispersion requirement in the generation of chirped RF signals based on frequency-to-time mapping," *Opt. Commun.*, vol. 331, pp. 278–281, Nov. 2014.

[33] L. R. Chen, "Silicon photonics for microwave photonics applications," *J. Lightw. Technol.*, vol. 35, no. 4, pp. 824–835, Feb. 2017.

[34] W. Zhang and J. Yao, "Silicon-based integrated microwave photonics," *IEEE J. Quantum Electron.*, vol. 52, no. 1, Jan. 2016, Art. no. 0600412.

[35] D. E. Leaird and A. M. Weiner, "Femtosecond direct space-to-time pulse shaping in an integrated-optic configuration," *Opt. Lett.*, vol. 29, no. 13, pp. 1551–1553, Jan. 2004.

[36] M. H. Khan *et al.*, "Ultrabroadbandwidth arbitrary radiofrequency waveform generation with a silicon photonic chip-based spectral shaper," *Nature Photon.,* vol. 4, pp. 117–122, Jan. 2010.

[37] W. Zhang, J. Zhang, and J. Yao, "Largely chirped microwave waveform generation using a silicon-based on-chip optical spectra shaper," in *Proc. Int. Topical Meeting Microw. Photon./9th Asia-Pacific Microw. Photon. Conf.*, 2014, pp. 51–53.

[38] J. Wang *et al.*, "Reconfigurable radio-frequency arbitrary waveforms synthesized in a silicon photonic chip," *Nature Commun.*, vol. 6, pp. 5957, Jan. 2015.

[39] Y. A. Vlasov and S. J. McNab, "Losses in single-mode silicon-on-insulator strip waveguides and bends," *Opt. Exp.*, vol. 12, no. 8, pp. 1622–1631, Apr. 2004.

[40] S. Xiao, M. H. Khan, H. Shen, and M. Qi, "Compact silicon microring resonators with ultra-low propagation loss in the C band," *Opt. Exp.*, vol. 15, no. 22, pp. 14467–14475, Oct. 2007.

[41] M. Ma and L. R. Chen, "Generating chirped microwave pulses using an integrated distributed Fabry–Pérot cavity in silicon-on-insulator," *IEEE Photon. J.*, vol. 7, no. 2, Apr. 2015.

[42] J. Wang, R. Ashrafi, M. Rochette, and L. R. Chen, "Chirped microwave pulse generation using an integrated silicon photonic spectral shaper," *IEEE Photon. Technol. Lett.*, vol. 27, no. 17, pp. 1876–1879, Sep. 2015.

[43] W. Zhang and J. Yao, "Photonic generation of linearly chirped microwave waveforms using a silicon-based on-chip spectral shaper incorporating two linearly chirped waveguide Bragg gratings," *J. Lightw. Technol.*, vol. 33, no. 24, pp. 5047–5054, Dec. 2015.

[44] W. Zhang and J. Yao, "Silicon-based on-chip electrically-tunable spectral shaper for continuously tunable linearly chirped microwave waveform generation," *J. Lightw. Technol.*, vol. 34, no. 20, pp. 4664–4672, Oct. 2016.

[45] H. Chi and J. Yao, "All-fiber chirped microwave pulse generation based on spectral shaping and wavelength-to-time conversion," *IEEE Trans. Microw. Theory Techn.*, vol. 55, no. 9, pp. 1958–1963, Sep. 2007.

[46] H. Chi and J. Yao, "Chirped RF pulse generation based on optical frequency-to-time mapping using a nonlinearly chirped fiber Bragg grating," *J. Lightw. Technol.*, vol. 26, no. 10, pp. 1282–1287, May 2008.

[47] C. Wang and J. Yao, "Photonic generation of chirped millimeter-wave pulses based on nonlinear frequency-to-time mapping in a nonlinearly chirped fiber Bragg grating," *IEEE Trans. Microw. Theory Techn.*, vol. 56, no. 2, pp. 542–553, Feb. 2008.

[48] R. Ashrafi, Y. Park, and J. Azaña, "Fiber-based photonic generation of high-frequency microwave pulses with reconfigurable linear chirp control," *IEEE Trans. Microw. Theory Techn.*, vol. 58, no. 11, pp. 3312–3319, Nov. 2010.

[49] M. A. Muriel, J. Azaña, and A. Carballar, "Real-time Fourier transformer based on fiber gratings," *Opt. Lett.*, vol. 24, no. 1, pp. 1–3, Feb. 1999.

[50] B. H. Kolner, "Space-time duality and the theory of temporal imaging," *IEEE J. Quantum Electron.*, vol. 30, no. 8, pp. 1951–1963, Aug. 1994.

[51] J. Azaña and M. A. Muriel, "Temporal self-imaging effects: Theory and application for multiplying pulse repetition rates," *IEEE J. Sel. Topics Quantum Electron.*, vol. 7, no. 4, pp. 728–744, Jul./Aug. 2001.

[52] J. Lancis, J. Caraquitena, P. Andres, and M. A. Muriel, "Temporal self-imaging effect for chirped laser pulse sequences: Repetition rate duty cycle tunability," *Opt. Commun.*, vol. 253, no. 1-3, pp. 156–163, Sep. 2005.

[53] A. M. Weiner, *Ultrafast Optics*. New York, NY, USA: Wiley, 2009.

[54] White paper, "Dispersion trimming using the programmable group delay capability of the waveshaper family of programmable optical processors," [Online]. Available: https://www.finisar.com/sites/default/files/resources/white_paper_waveshaper_ dispersion_trimming.pdf

[55] S. Lee *et al.*, "Adjustable compensation of polarization mode dispersion using a high-birefringence, nonlinearly chirped fiber Bragg grating," *IEEE Photon. Technol. Lett.*, vol. 11, no. 10, pp. 1277–1279, Oct. 1999.

[56] Z. Pan *et al.*, "Tunable chromatic dispersion compensation in 40 Gbit/s systems using nonlinearly chirped fiber Bragg grating," *J. Lightw. Technol.*, vol. 20, no. 12, pp. 2239–2246, Dec. 2002.

[57] J. J. O'Reilly, P. M. Lane, R. Heidemann, and R. Hofstetter, "Optical generation of very narrow linewidth millimeter wave signals," *Electron. Lett.*, vol. 28, no. 25, pp. 2309–2311, Dec. 1992.

[58] G. Qi, J. Yao, J. Seregelyi, C. Bélisle, and S. Paquet, "Generation and distribution of a wide-band continuously tunable mm-wave signal with an optical external modulation technique," *IEEE Trans. Microw. Theory Techn.*, vol. 53, no. 10, pp. 3090–3097, Oct. 2005.

[59] G. Qi, J. Yao, J. Seregelyi, C. Bélisle, and S. Paquet, "Optical generation and distribution of continuously tunable millimeter-wave signals using an optical phase modulator," *J. Lightw. Technol.*, vol. 23, no. 9, pp. 2687–2695, Sept. 2005.

[60] Y. Li, J. Li, Y. Wang, and J. Yuan, "Filter-less frequency doubling microwave signal generator with tunable phase shift," *Opt. Commun.*, vol. 370, pp. 91–97, Jul. 2016.

[61] R. Li *et al.*, "Demonstration of a microwave photonic synthetic aperture radar based on photonic-assisted signal generation and stretch processing," *Opt. Exp.*, vol. 25, no. 13, pp. 14334–14340, Jun. 2017.

[62] F. Zhang *et al.*, "Photonics-based broadband radar for high-resolution and real-time inverse synthetic aperture imaging," *Opt. Exp.*, vol. 25, no. 14, pp. 16274–16281, Jul. 2017.

[63] D. Zhu and J. Yao, "Dual-chirp microwave waveform generation using a dual-parallel Mach–Zehnder modulator," *IEEE Photon. Technol. Lett.*, vol. 27, no. 13, pp. 1410–1413, Jul. 2015.

[64] Y. Xu, T. Jin, H. Chi, S. Zheng, X. Jin, and X. Zhang, "Photonic generation of dual-chirp waveforms with improved time bandwidth product," *IEEE Photon. Technol. Lett.*, vol. 29, no. 15, pp. 1253–1256, Aug. 2017.

[65] A. Amar and Y. Buchris, "Asynchronous transmitter position and velocity estimation using a dual linear chirp," *IEEE Signal Process. Lett.*, vol. 21, no. 9, pp. 1078–1082, Sept. 2014.

[66] F. Coppinger, A. S. Bhushan, and B. Jalali, "Photonic time stretch and its application to analog-to-digital conversion," *IEEE Trans. Microw. Theory Techn.*, vol. 47, no. 7, pp. 1309–1314, Jul. 1999.

[67] Y. Han, O. Boyraz, and B. Jalali, "Tera-sample per second real-time waveform digitizer," *Appl. Phys. Lett.*, vol. 87, no. 24, Sep. 2005.

[68] F. Coppinger, A. S. Bhushan, and B. Jalali, "Time reversal of broadband microwave signals," *Electron. Lett.*, vol. 35, no. 15, pp. 1230–1232, Jul. 1999.

[69] J. U. Kang, M. Y. Frankel, and R. D. Esman, "Demonstration of microwave frequency shifting by use of a highly chirped mode-locked fiber laser," *Opt. Lett.*, vol. 23, no. 15, pp. 1188–1190, Aug. 1998.

[70] C. Wang, M. Li, and J. Yao, "Continuously tunable photonic microwave frequency multiplication by use of an unbalanced temporal pulse shaping system," *IEEE Photon. Technol. Lett.*, vol. 22, no. 17, pp. 1285–1287, Sep. 2010.

[71] M. Li, C. Wang, W. Li, and J. Yao, "An unbalanced temporal pulse-shaping system for chirped microwave waveform generation," *IEEE Trans. Microw. Theory Techn.*, vol. 58, no. 11, pp. 2968–2975, Nov. 2010.

[72] J. Azaña, N. K. Berger, B. Levit, and B. Fischer, "Broadband arbitrary waveform generation based on microwave frequency upshifting in optical fibers," *J. Lightw. Technol.*, vol. 24, no. 7, pp. 2663–2675, Jul. 2006.

[73] B. Xu, C. Liu, X. Jin, H. Chi, S. Zheng, and X. Zhang, "Time-division multiplexed vector signal synthesizer based on continuous PTS," *IEEE Photon. Technol. Lett.*, vol. 30, no. 11, pp. 1020–1023, Jun. 2018.

[74] Y. Han and B. Jalali, "Time-bandwidth product of the photonic time stretched analog-to-digital converter," *IEEE Trans. Microw. Theory Techn.*, vol. 51, pp. 1886–1892, Jul. 2003.

[75] Y. Han, O. Boyraz, and B. Jalali, "Ultrawide-band photonic time-stretch A/D converter employing phase diversity," *IEEE Trans. Microw. Theory Techn.*, vol. 53, no. 4, pp. 1404–1408, Apr. 2005.

[76] X. S. Yao and L. Maleki, "Converting light into spectrally pure microwave oscillation," *Opt. Lett.*, vol. 21, no. 7, pp. 483–485, Apr. 1996.

[77] X. S. Yao and L. Maleki, "Optoelectronic microwave oscillator," *J. Opt. Soc. Amer. B*, vol. 13, no. 8, pp. 1725–1735, Dec. 1996.

[78] B. Yang *et al.*, "A tunable optoelectronic oscillator based on a dispersion-induced microwave photonic filter," *IEEE Photon. Technol. Lett.*, vol. 25, no. 10, pp. 921–924, May 2013.

[79] J. Yao, "Optoelectronic oscillators for high speed and high resolution optical sensing," *J. Lightw. Technol.*, vol. 35, no. 16, pp. 3489–3497, Aug. 2017.

[80] D. Eliyahu *et al.*, "Resonant widely tunable opto-electronic oscillator," *IEEE Photon. Technol. Lett.*, vol. 25, no. 15, pp. 1535–1538, Aug. 2013.

[81] R. Huber, M. Wojtkowski, and J. G. Fujimoto, "Fourier domain mode locking (FDML): A new laser operating regime and applications for optical coherence tomography," *Opt. Exp.*, vol. 14, no. 8, pp. 3225–3237, Apr. 2006.

[82] T. Hao *et al.*, "Breaking the limitation of mode building time in an optoelectronic oscillator," *Nature Commun.,* vol. 9, pp. 19839, May 2018.

[83] T. Hao, J. Tang, N. Shi, W. Li, N. Zhu, and M. Horowitz, "Dual-chirp Fourier domain mode-locked optoelectronic oscillator," *Opt. Lett.*, vol. 44, no. 8 pp. 1912–1915, Apr. 2019.

[84] T. Hao, J. Tang, W. Li, N. Zhu, and M. Li, "Fourier domain mode locked optoelectronic oscillator based on the deamplification of stimulated brillouin scattering," *OSA Continuum*, vol. 1, no. 2, pp. 408–415, 2018.

[85] T. Hao, J. Tang, W. Li, N. Zhu, and M. Li, "Tunable Fourier domain mode-locked optoelectronic oscillator using stimulated brillouin scattering," *IEEE Photon. Technol. Lett.*, vol. 30, no. 21, pp. 1842–1845, Nov. 2018.

[86] P. Hao, H. Lu, R. Han, X. Wang, X. Liu, and X. S. Yao, "Fourier domain mode-locked opto-electronic oscillator with a diode-tuned bandpass filter," *Opt. Exp.*, vol. 28, no. 16, pp. 23454–23466, Jul. 2020.

[87] J. W. Shi, F. M. Kuo, N. W. Chen, S. Y. Set, C. B. Huang, and J. E. Bowers, "Photonic generation and wireless transmission of linearly/nonlinearly continuously chirped millimeter-wave waveforms with high time-bandwidth product at W-band," *IEEE Photon. J.,* vol. 4, no. 1, pp. 215–223, Feb. 2012.

[88] J. M. Wun, C. C. Wei, J. Chen, C. S. Goh, S. Y. Set, and J. W. Shi, "Photonic chirped radio-frequency generator with ultra-fast sweeping rate and ultra-wide sweeping range," *Opt. Exp.*, vol. 21, no. 9, pp. 11475–11481, May 2013.

[89] H. Gao, C. Lei, M. Chen, F. Xing, H. Chen, and S. Xie, "A simple photonic generation of linearly chirped microwave pulse with large time-bandwidth product and high compression ratio," *Opt. Exp.*, vol. 21, no. 20, pp. 23107–23115, Oct. 2013.

[90] J. Tang, B. Zhu, M. Li, S. Pan, and J. Yao, "Hybrid Fourier-domain mode-locked laser for ultra-wideband linearly chirped microwave waveform generation," *Nature Commun.,* vol. 11, pp. 3814, Jul. 2020.

[91] Y. Dai and J. Yao, "Chirped microwave pulse generation using a photonic microwave delay-line filter with a quadratic phase response," *IEEE Photon. Technol. Lett.*, vol. 21, no. 9, pp. 569–571, May 2009.

[92] P. Zhou, F. Zhang, Q. Guo, and S. Pan, "Linearly chirped microwave waveform generation with large time-bandwidth product by optically injected semiconductor laser," *Opt. Exp.*, vol. 24, no. 16, pp. 18460–18467, Aug. 2016.
[93] P. Del'Haye, A. Schliesser, O. Arcizet, T. Wilken, R. Holzwarth, and T. Kippenberg, "Optical frequency comb generation from a monolithic microresonator," *Nature*, vol. 450, pp. 1214–1217, Dec. 2007.
[94] S. Pan and Y. Zhang, "Microwave photonic radars," *J. Lightw. Technol.*, vol. 38, no. 19, pp. 5450–5480, Oct. 2020.
[95] M. Gagné, S. Loranger, J. Lapointe, and R. Kashyap, "Fabrication of high quality, ultra-long fiber Bragg gratings: Up to 2 million periods in phase," *Opt. Exp.*, vol. 22, no. 1, pp. 387–398, Jan. 2014.

HAO CHI (Senior Member, IEEE) received the B.S. degree in applied physics from Xi'an Jiaotong University, Xi'an, China, in 1994 and the Ph.D. degree in electronic engineering from Zhejiang University, Hangzhou, China, in 2001. He is currently a Professor with the School of Communication Engineering, Hangzhou Dianzi University, Hangzhou, China.

From 2000 to 2001, he was a Research Assistant with The Hong Kong Polytechnic University, Hong Kong. From 2001 to 2003, he was a Postdoctoral Research Fellow with the Department of Electronic Engineering, Shanghai Jiao Tong University, Shanghai, China. From 2003 to 2018, he was with the College of Information Science and Electronic Engineering, Zhejiang University, Hangzhou, China, where he became a Full Professor in 2008. From 2006 to 2008, he was a Visiting Professor with the Microwave Photonics Research Laboratory, School of Information Technology and Engineering, University of Ottawa, Ottawa, ON, Canada. He has authored and coauthored more than 140 research papers in peer-reviewed journals. His research interests include microwave photonics, optical signal processing, and optical communications. He is currently an Associate Editor for IEEE PHOTONICS TECHNOLOGY LETTERS.

CHAO WANG (Senior Member, IEEE) received the B.Eng. degree in optoelectrical engineering from Tianjin University, Tianjin, China, in 2002, the M.Sc. degree in optics from Nankai University, Tianjin, China, in 2005, and the Ph.D. degree in electrical and computer engineering from the University of Ottawa, Ottawa, ON, Canada, in 2011.

From 2011 to 2012, he was appointed Postdoctoral Fellow with Photonics Laboratory, the University of California, Los Angeles, Los Angeles, CA, USA. In 2013, he was a Lecturer with the School of Engineering and Digital Arts, University of Kent, Canterbury, U.K., where he became a Senior Lecturer in 2017. His research interests include microwave photonics, ultrafast imaging, optical communications, optical sensing, and biophotonics for scientific and engineering applications.

Dr. Wang was the recipient of the IEEE Photonics Society Graduate Student Fellowship in 2009, the IEEE MTT-S Graduate Fellowship in 2010, the Vanier Canada Graduate Scholarship in 2009, the Chinese Government Award for Outstanding Self-Financed Students Abroad in 2009, the Natural Sciences and Engineering Research Council of Canada Postdoctoral Fellowship in 2010, and was awarded the EU FP-7 Marie-Curie Career Integration Grant in 2014. He is an Associate Editor for IEEE PHOTONICS TECHNOLOGY LETTERS.

JIANPING YAO (Fellow, IEEE) received the Ph.D. degree in electrical engineering from the Université de Toulon et du Var, Toulon, France, in December 1997. He is currently a Distinguished University Professor and the University Research Chair with the School of Electrical Engineering and Computer Science, University of Ottawa, Ottawa, ON, Canada. From 1998 to 2001, he was with the School of Electrical and Electronic Engineering, Nanyang Technological University, Singapore, as an Assistant Professor. In December 2001, he joined the School of Electrical Engineering and Computer Science, University of Ottawa, as an Assistant Professor, where he was promoted to an Associate Professor in May 2003, and a Full Professor in May 2006. In 2017, he was appointed University Research Chair of Microwave Photonics. In June 2016, he was conferred the title of Distinguished University Professor with the University of Ottawa. From July 2007 to June 2010 and July 2013 to June 2016, he was the Director of the Ottawa-Carleton Institute for Electrical and Computer Engineering, Ottawa, ON, Canada.

He has authored or coauthored more than 620 research papers, including more than 360 papers in peer-reviewed journals and more than 260 papers in conference proceedings. He is the Editor-in-Chief of IEEE PHOTONICS TECHNOLOGY LETTERS, the former Topical Editor of *Optics Letters*, an former Associate Editor for the *Science Bulletin*, a Steering Committee Member of IEEE JOURNAL OF LIGHTWAVE TECHNOLOGY, and an Advisory Editorial Board Member of *Optics Communications*. He was the Guest Editor of the Focus Issue on Microwave Photonics in Optics Express in 2013, the Lead-Editor of a Feature Issue on *Microwave Photonics* in Photonics Research in 2014, and a Guest Editor of a special issue on Microwave Photonics in IEEE/OSA JOURNAL OF LIGHTWAVE TECHNOLOGY in 2018. He is currently the Technical Committee Chair of IEEE MTT-S Microwave Photonics and an elected Member of the Board of Governors of the IEEE Photonics Society from 2019 to 2021. He was a Member of the European Research Council Consolidator Grant Panel in 2016, 2018, and 2020, the Qualitative Evaluation Panel in 2017, and a panelist of the National Science Foundation Career Awards Panel in 2016. He was the Chair of a number of international conferences, symposia, and workshops, including the Vice Technical Program Committee (TPC) Chair of the 2007 IEEE Topical Meeting on Microwave Photonics, TPC Co-Chair of the 2009 and 2010 Asia-Pacific Microwave Photonics Conference, TPC Chair of the high-speed and broadband wireless technologies subcommittee of the IEEE Radio Wireless Symposium 2009–2012, TPC Chair of the microwave photonics subcommittee of the IEEE Photonics Society Annual Meeting 2009, TPC Chair of the 2010 IEEE Topical Meeting on Microwave Photonics, General Co-Chair of the 2011 IEEE Topical Meeting on Microwave Photonics, TPC Co-Chair of the 2014 IEEE Topical Meetings on Microwave Photonics, General Co-Chair of the 2015 and 2017 IEEE Topical Meeting on Microwave Photonics, and General Chair of the 2019 IEEE Topical Meeting on Microwave Photonics. He was also a Committee Member for a number of international conferences, including IPC, OFC, CLEO, BGPP, and MWP. He was the recipient of the 2005 International Creative Research Award of the University of Ottawa, the 2007 George S. Glinski Award for Excellence in Research, the Natural Sciences and Engineering Research Council of Canada Discovery Accelerator Supplements Award in 2008, an inaugural OSA Outstanding Reviewer Award in 2012 and was one of the top ten reviewers of IEEE/OSA JOURNAL OF LIGHTWAVE TECHNOLOGY from 2015 to 2016, the 2017–2018 Award for Excellence in Research of the University of Ottawa, and the 2018 R.A. Fessenden Silver Medal from IEEE Canada. From 2013 to 2015, he was an IEEE MTT-S Distinguished Microwave Lecturer.

He is currently a registered Professional Engineer of Ontario. He is a Fellow of the Optical Society of America (OSA), the Canadian Academy of Engineering, and the Royal Society of Canada.